


















Dynamical Architectures of S-type Transiting Planets in Binaries I: Target Selection using Hipparcos and Gaia proper motion anomalies*

JINGWEN ZHANG (张婧雯) ^{1, †} LAUREN M. WEISS ² DANIEL HUBER ¹ ERIC L. N. JENSEN ³
TIMOTHY D. BRANDT ⁴ KAREN COLLINS ⁵ DENNIS M. CONTI ⁶ HOWARD ISAACSON ^{7, 8} PABLO LEWIN ⁹
GUISEPPI MARINO ^{10, 11} BOB MASSEY ¹² FELIPE MURGAS ^{13, 14} ENRIC PALLE ^{13, 14} DON J. RADFORD ¹⁵
HOWARD M. RELLES,⁵ GREGOR SRDOC,¹⁶ CHRIS STOCKDALE ¹⁷ THIAM-GUAN TAN ¹⁸ AND GAVIN WANG ¹⁹

¹*Institute for Astronomy, University of Hawai'i, Honolulu, HI 96822, USA*

²*Department of Physics, University of Notre Dame*

334 Nieuwland Science Hall, Notre Dame, IN 46556, USA

³*Department of Physics & Astronomy, Swarthmore College, Swarthmore PA 19081, USA*

⁴*Department of Physics, University of California, Santa Barbara, Santa Barbara, CA 93106, USA*

⁵*Center for Astrophysics | Harvard & Smithsonian, 60 Garden Street, Cambridge, MA 02138, USA*

⁶*American Association of Variable Star Observers, 185 Alewife Brook Parkway, Suite 410, Cambridge, MA 02138, USA*

⁷*501 Campbell Hall, University of California at Berkeley, Berkeley, CA 94720, USA*

⁸*Centre for Astrophysics, University of Southern Queensland, Toowoomba, QLD, Australia*

⁹*The Maury Lewin Astronomical Observatory, Glendora, California. 91741, USA*

¹⁰*Wild Boar Remote Observatory, San Casciano in val di Pesa, Firenze, 50026 Italy*

¹¹*INAF - Osservatorio Astrofisico di Catania, Via S. Sofia 78, 95123 Catania, Italy*

¹²*Villa '39 Observatory, Landers, CA 92285, USA*

¹³*Instituto de Astrofísica de Canarias (IAC), E-38205 La Laguna, Tenerife, Spain*

¹⁴*Departamento de Astrofísica, Universidad de La Laguna (ULL), E-38206 La Laguna, Tenerife, Spain*

¹⁵*American Association of Variable Star Observers, 49 Bay State Road, Cambridge, MA 02138, USA*

¹⁶*Kotizarovci Observatory, Sarsoni 90, 51216 Viskovo, Croatia*

¹⁷*Hazelwood Observatory, Australia*

¹⁸*Perth Exoplanet Survey Telescope, Perth, Western Australia*

¹⁹*Tsinghua International School, Beijing 100084, China*

(Received June 1, 2022; Revised June 1, 2022; Accepted March 6, 2024)

ABSTRACT

The effect of stellar multiplicity on planetary architecture and orbital dynamics provides an important context for exoplanet demographics. We present a volume-limited catalog up to 300 pc of 66 stars hosting planets and planet candidates from *Kepler*, *K2* and *TESS* with significant Hipparcos-Gaia proper motion anomalies, which indicates the presence of companions. We assess the reliability of each transiting planet candidate using ground-based follow-up observations, and find that the TESS Objects of Interest (TOIs) with significant proper anomalies show nearly four times more false positives due to Eclipsing Binaries compared to TOIs with marginal proper anomalies. In addition, we find tentative evidence that orbital periods of planets orbiting TOIs with significant proper anomalies are shorter than those orbiting TOIs without significant proper anomalies, consistent with the scenario that stellar companions can truncate planet-forming disks. Furthermore, TOIs with significant proper anomalies exhibit lower Gaia differential velocities in comparison to field stars with significant proper anomalies, suggesting that planets are more likely to form in binary systems with low-mass substellar companions or stellar companions at wider separation. Finally, we characterize the three-dimensional architecture of LTT 1445 ABC using radial velocities, absolute astrometry from Gaia and Hipparcos, and relative astrometry from imaging. Our analysis reveals that LTT 1445 is a nearly flat system, with a mutual

Corresponding author: Jingwen Zhang

jingwen7@hawaii.edu

* Also referred to as Hipparcos and Gaia astrometric accelerations

inclination of $\sim 2.88^\circ$ between the orbit of BC around A and that of C around B. The coplanarity may explain why multiple planets around LTT1445 A survive in the dynamically hostile environments of this system.

Keywords: editorials, notices — miscellaneous — catalogs — surveys

1. INTRODUCTION

Radial velocity (RV, Cumming et al. 2008; Fulton et al. 2021) surveys and space-based transit searches such as *Kepler* (Borucki et al. 2010; Howard et al. 2012) and *TESS* (Ricker et al. 2014) have revolutionized our understanding of exoplanet demographics. However, the process of confirming exoplanets is biased against stars in multiple systems, since close companions complicate the observations and analysis. Although one third of nearby solar-type stars have at least one companion (Raghavan et al. 2010), the effects of stellar multiplicity on planetary architecture and orbital dynamics are still poorly understood. In addition, unknown stellar companions can cause inaccuracy for estimating planet radius by diluting the measured transit depths (Furlan et al. 2017; Teske et al. 2018; Sullivan et al. 2023). Planet properties may also be inaccurate if the planet is actually orbiting the secondary star. Thus, identifying the stellar companions of transiting planets helps to obtain more accurate planet parameters and characterize the demographics of planets in binaries (Fontanive & Bardalez Gagliuffi 2021; Cadman et al. 2022). By analyzing large samples of planets in binaries and comparing them to single systems, we can gain insights into the factors that shape the the formation and evolution of exoplanets.

Close companions are expected to have a deleterious influence on planet formation, through disk truncation (Artymowicz & Lubow 1994; Jang-Condell et al. 2015) or dynamical stirring of planetesimals (Quintana et al. 2007). Recent ALMA observations show that disks in binaries have lower masses (Akeson et al. 2019) and smaller radii (Cox et al. 2017; Manara et al. 2019), supporting the disk truncation scenario. Kraus et al. (2016) used high-resolution adaptive optics (AO) imaging of 382 Kepler Objects of Interest (KOIs) to show that planet occurrence rate in close binaries (< 47 AU) is only 0.34 times that of single stars or wide binaries. Ziegler et al. (2020, 2021); Howell et al. (2021); Lester et al. (2021) performed similar searches for stellar companions to TESS Objects of Interest (TOIs) and also found a deficit of close binaries (< 100 AU). For giant planets discovered by RV observations, Hirsch et al.

(2021) reported that the planet occurrence rate in binaries with a separation < 100 AU is significantly smaller than those in binaries with a separation > 100 AU or single stars. Additionally, Fontanive & Bardalez Gagliuffi (2021) presents a volume-limited sample of companions from tens of AU out to 20000 AU in the literature and Gaia DR2 to exoplanet host stars. They found giant planets with masses above $0.1 M_J$ are more frequently seen than small sub-Jovian planets in binary systems, which is supported by the simulations from Cadman et al. 2022.

However, some planets survive in such dynamically challenging environments for reasons that are still unclear (Hatzes et al. 2003; Correia et al. 2008; Kane et al. 2015; Dupuy et al. 2016). Close binary companions could induce gravitational perturbations on their orbits, causing the migration or spin-orbit misalignment of planets. Furthermore, close companions may torque the protoplanetary disks where planets form, and therefore shape the architecture of the planet systems. Studying the architecture of planets in close binary systems will shed light on the planet formation and evolution in these systems.

Transit surveys including *TESS*, *Kepler* and *K2* offer an unbiased planet sample in terms of stellar multiplicity. The coarse spatial resolution of *TESS* ($21''/\text{pixel}$) and *Kepler* ($4''/\text{pixel}$) makes it essential to conduct ground-based follow-up observations to resolve close binary systems. Previous studies have used adaptive optics (AO) and speckle imaging to search for stellar companions to planet candidate hosts discovered by *Kepler* and *TESS* missions (Kraus et al. 2016; Ziegler et al. 2020, 2021; Howell et al. 2021; Lester et al. 2021). *Gaia* mission’s Renormalised Unit Weight Error (RUWE) is also an indicator for companions, as RUWE values are sensitive to the deviation from the single-star astrometric model. However, RUWE values are most effective for detecting binaries with separations from $0''.1$ to $0''.6$ (Lindgren et al. 2018; Ziegler et al. 2020). The companions located outside of the range might be overlooked.

In this paper, we use *Gaia* (Gaia Collaboration et al. 2022) and *Hipparcos* (ESA 1997) proper motion anomalies (Kervella et al. 2019; Brandt et al. 2019) to identify close companions hiding in the large pixels of *TESS* or *Kepler*. The method takes advantage of ~ 25 years time baseline between the two missions, and is sensitive to

† NASA FINESST Fellow

companions with orbital periods from decades to centuries (Kervella et al. 2019). Furthermore, the combination of *Gaia* and *Hipparcos* astrometry, radial velocities (RVs) and imaging astrometry makes it possible to determine the 3D orbits of the companions and obtain their dynamical masses (Brandt et al. 2019; Xuan & Wyatt 2020). In this paper, we characterized the 3D orbits of companions in the proof-of-concept system LTT 1445 ABC with the method. It's important to note that our emphasis here is on the orbit parameters of stellar companions with orbital periods in years, rather than on transiting planets with much shorter orbital periods in the order of days. Finally, By obtaining the inclinations of the companion orbits, we can constrain the mutual inclinations between the orbital plane of the companion and that of the transiting planet. This information can provide insight into the system's dynamical history.

2. HIPPARCOS-GAIA PROPER MOTION ANOMALIES

The *Gaia* spacecraft (Gaia Collaboration et al. 2022) measures the position and proper motion of nearly 1.7 billion stars since 2014. Its predecessor *Hipparcos* (Perryman et al. 1997) also provides precise astrometric measurements of nearby stars from 1989 to 1993. The measurements have a time baseline of nearly 25 years and can detect the effect of unresolved binaries since a companion would cause the primary to wobble around the barycenter on the sky plane (Brandt et al. 2019; Kervella et al. 2019). Specifically, we use *Hipparcos* and *Gaia* EDR3 proper motions and their uncertainties from the Hipparcos-Gaia Catalog of Accelerations (HGCA, Brandt 2021). The catalog provides three proper motions for every star: (1) the *Hipparcos* proper motion μ_H at an epoch near 1991.25; (2) the *Gaia* EDR3 proper motion μ_G at an epoch near 2016.01; (3) long-term proper motion μ_{HG} given by position difference between *Hipparcos* and *Gaia* divided by the 25 years baseline.

These proper motions are in units of mas yr^{-1} . The proper motions are given in right ascension (RA, α) and declination (DEC, δ) direction. For simplicity, we use the total proper motion combined from the two directions and omit the subscript for RA and DEC in this paper. The long-term proper motion μ_{HG} can be used to estimate the velocity of celestial linear motion across the sky plane over nearly 25 years. We subtracted the long-term proper motion μ_{HG} from *Hipparcos* and *Gaia* proper motions as follows:

$$\begin{aligned}\Delta\mu_H &= \mu_H - \mu_{HG} \\ \Delta\mu_G &= \mu_G - \mu_{HG}\end{aligned}\quad (1)$$

The two residuals represent the proper motion anomalies at the *Hipparcos* and *Gaia* epochs, respectively (Kervella et al. 2019). Note that these anomalies are also known as astrometric accelerations (Brandt 2021). We use the terminology of "proper motion anomalies" to prevent confusion with the general concept of "acceleration," as the residuals are measured in the unit of mas year^{-1} .

As shown in Figure 1, a significant proper motion anomalies reveals a deviation from the linear stellar motion, possibly caused by a gravitationally bound companion. We calculate the signal-to-noise ratio of proper motion anomalies at *Hipparcos* and *Gaia* epochs using the calibrated uncertainties of *Hipparcos* and *Gaia* measurements from Brandt (2021):

$$\begin{aligned}\text{SNR}_G &= \frac{\mu_G - \mu_{HG}}{\sqrt{\sigma[\mu_G]^2 + \sigma[\mu_{HG}]^2}} \\ \text{SNR}_H &= \frac{\mu_H - \mu_{HG}}{\sqrt{\sigma[\mu_H]^2 + \sigma[\mu_{HG}]^2}}\end{aligned}\quad (2)$$

where $\sigma[\mu]$ represent the uncertainties.

Next, we convert the proper motion anomalies in the unit of mas yr^{-1} into the differential velocities in the unit of $m s^{-1}$ as follows (Kervella et al. 2019):

$$\begin{aligned}\Delta v_G [m s^{-1}] &= \frac{\Delta\mu_G [\text{mas yr}^{-1}]}{\varpi [\text{mas}]} \times 4740.47 \\ \Delta v_H [m s^{-1}] &= \frac{\Delta\mu_H [\text{mas yr}^{-1}]}{\varpi [\text{mas}]} \times 4740.47\end{aligned}\quad (3)$$

where ϖ is the parallax in units of mas . For a binary system, the differential velocity is approximately the projected tangential velocities of the primary's orbital motion on the sky plane (Kervella et al. 2019). Based on Kepler's law, the differential velocities are proportional to the companion masses (m_c) and inversely proportional to the square root of orbital distances (r): $\Delta v \propto \frac{m_c}{\sqrt{r}}$. Due to the observing window smearing effect (for details see Kervella et al. 2019), the proper motion anomalies method is most sensitive to companions with orbital periods longer than observing windows of *Hipparcos* and *Gaia* ($\delta_H = 1227$ days, Perryman et al. 1997, $\delta_{G,DR3} = 1038$ days, Gaia Collaboration et al. 2022). On the other hand, the efficiency of the proper motion anomalies method drops for companions at orbital periods much longer than the 25-year baseline between the two missions. For instance, the efficiency is reduced to $\sim 30\%$ when the orbital period is ten times the time baseline (~ 250 years) (Kervella et al. 2019). Therefore, the sweet spot of proper motion anomalies is for companions at orbital periods from ~ 3 years up

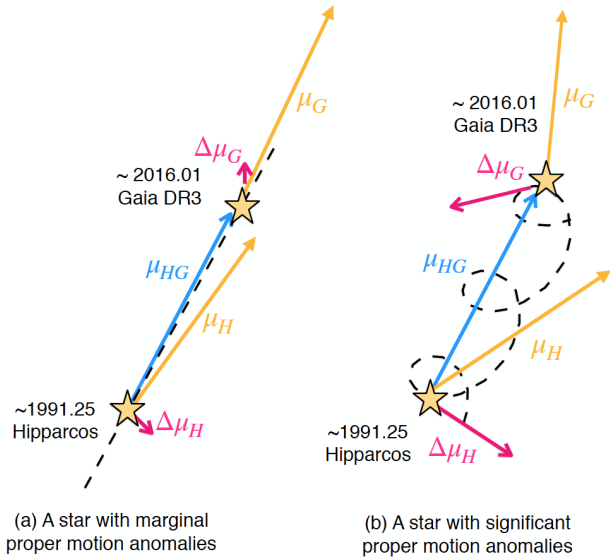


Figure 1. Principle of Hipparcos Gaia proper motion anomalies. μ_H and μ_G represent the proper motions of the same star measured by Hipparcos and Gaia with a time baseline of around 25 years. μ_{HG} is the stellar long-term velocity across the sky plane. If we subtract μ_{HG} from μ_H and μ_G , the residuals are the proper motion anomalies at Hipparcos and Gaia epochs, respectively. (a) A star with marginal proper motion anomalies: if μ_H and μ_G are similar to the long-term velocity μ_{HG} , the star moves across the sky plane in a linear motion. (b) A star with significant proper motion anomalies: a significant residual indicates the star not only moves linearly but also orbits around the system barycenter due to the gravitational pull from a companion.

to ~ 250 years, corresponding to a few AU to dozens of AU in terms of the semi-major axis. Multiple studies have found a deficiency of planets in close binaries with separation below 100 AU, supporting the theory of close companions disturbing and preventing planet formation (Kraus et al. 2016; Ziegler et al. 2020; Hirsch et al. 2021; Fontanive & Bardalez Gagliuffi 2021; Cadman et al. 2022). *Hipparcos* and *Gaia* astrometry thus offers an efficient way to search for planets in binaries that have separation of < 100 AU, with which we can study the effect of companions on planet formation and evolution.

3. TARGET SELECTION

3.1. Methodology

We constructed our target sample from host stars of transiting planet candidates, including TESS/Kepler Object of Interest (TOIs/KOIs) and K2 planet candidates. We used 4763 KOIs (2402 confirmed planets) from *Kepler* (Batalha et al. 2013; Burke et al. 2014; Rowe et al. 2015; Mullally et al. 2015; Coughlin et al. 2016; Thompson et al. 2018), 1547 K2 planet candidates

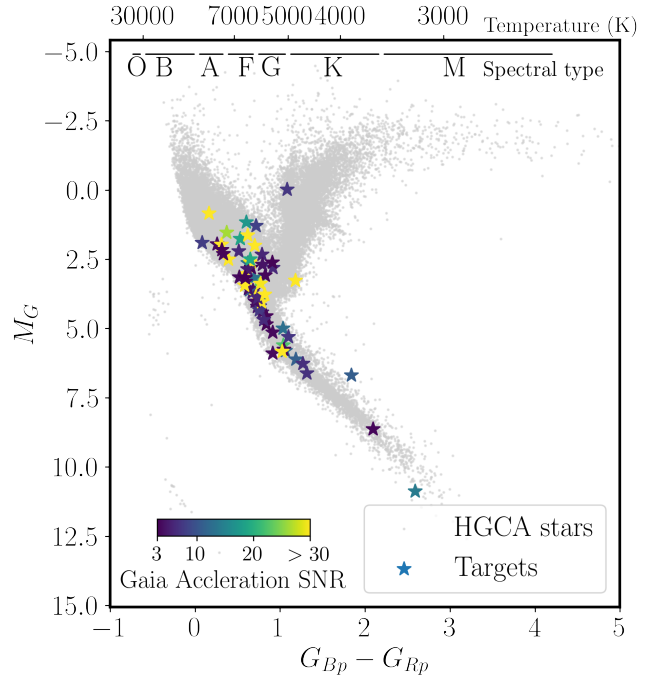


Figure 2. Gaia color-absolute magnitude diagram for our targets (star signs) and stars in HGCA within 300 pc (grey dots). TOI/KOI/K2 planet candidate hosts with significant proper motion anomalies are color-coded by the signal-to-noise ratio of their proper motion anomalies at Gaia epoch (SNR_G).

(569 confirmed planets) from *K2* mission (Howell et al. 2014; Huber et al. 2016; Pope et al. 2016; Kostov et al. 2019; Zink et al. 2021), and 6682 TOIs (360 confirmed planets) from *TESS* (Guerrero et al. 2021). We downloaded the TOI/KOI/K2 lists from NASA Exoplanet Archive¹. Next, we used the Hipparcos and Gaia proper motion anomalies as an indicator to search for hidden companions to the planet or planet candidate hosts. Our procedure for selecting targets is as follows:

1. We cross-matched KOI/K2/TOI lists with HGCA using their RA ($\Delta\alpha < 10''$), DEC ($\Delta\delta < 10''$), and parallax ($\Delta\varpi/\varpi_{\text{Gaia}} < 20\%$).
2. We calculated the distance of targets with *Gaia* DR3 parallax and selected stars with distances smaller than 300 pc.
3. We calculated the signal-to-noise of *Gaia* proper motion anomalies of every star from the last step. We selected those showing *Gaia* proper motion anomalies with $\geq 3\sigma$ significance ($\text{SNR}_G \geq 3$) into our target sample. Hereafter, we refer to our sam-

¹ <https://exoplanetarchive.ipac.caltech.edu/>

ple as HGCA-high-SNR stars or stars with significant proper motion anomalies.

4. We also constructed a control sample of TOI stars with $\text{SNR}_G < 3$. Hereafter, we refer to the control sample as HGCA-low-SNR stars or stars with marginal proper motion anomalies.

There are a total of 66 systems (58 TOIs, 4 KOIs, and 4 K2 planet candidates) in our target sample with high-SNR proper motion anomalies (see Table 1). We also identified 254 TOIs with low-SNR proper motion anomalies in the control sample and list them in Appendix C. The HGCA provides a parameter called χ^2 , which represents the chi-squared value obtained from fitting a constant proper motion to the more precise pair of $\mu_{\text{HG}} - \mu_G$ and $\mu_{\text{H}} - \mu_{\text{HG}}$ proper motion measurements (Brandt 2021). This parameter is also helpful in evaluating the significance of proper motion anomalies. For instance, a χ^2 value of 11.8 corresponds to a 3σ evidence for proper motion anomalies. We compare the output samples using criteria of $\chi^2 \geq 11.8$ and $\text{SNR}_G \geq 3$. The two criteria are nearly equivalent, resulting in comparable samples.

3.2. Target Sample

Figure 2 presents a color-absolute magnitude diagram of 66 selected targets (58 TOIs, 4 KOIs and 4 K2 planet candidates), color-coded by the significance of Hipparcos-Gaia proper motion anomalies. We calculated the absolute magnitude using $M_G = m_G + 5 \log d + 5$, where m_G and d are Gaia G band apparent magnitude and distance. Most of our targets are main sequence stars with $0.5 < G_{Bp} - G_{Rp} < 1.5$ and $0 < M_G < 7$. We highlight stars with multiple transiting planets in Table 1, including TOI-402 (Gandolfi et al. 2019; Dumusque et al. 2019), TOI-455 (LTT 1445 Winters et al. 2019, 2022), TOI-144 (π Men Jones et al. 2002; Gandolfi et al. 2018; Hatzes et al. 2022), TOI-201 (Hobson et al. 2021), TOI-1339 (HD 191939, Badenas-Agusti et al. 2020; Lubin et al. 2022; Orell-Miquel et al. 2023),

TOI-1730 (Simpson & Cloutier 2022), and KOI03158 (Kepler-444, Campante et al. 2015).

Some targets in our sample have been investigated before. The triple system Kepler-444 consists of a primary star with five transiting Mars-sized and Mars-mass planets. Dupuy et al. (2016) and Mills & Fabrycky (2017) characterized the Kepler-444 BC companion pair as orbiting the primary A in a highly eccentric orbit ($e \sim 0.864$, $a \sim 5$ AU) using RVs and relative astrometry from imaging. Recently, Zhang et al. (2022) improved the constraints on the orbit of the Kepler-444 BC pair ($e \sim 0.55$, $a \sim 36$ AU, $i \sim 85.4$ deg) using a longer time baseline of RVs and the proper motion anomalies data from the *Hipparcos* and *Gaia* missions. Both studies suggest that Kepler-444 BC may have truncated the protoplanetary disk of the primary, resulting in the small sizes of the system’s five planets. Zhou et al. (2022) characterizes the 3D orbit of an M-dwarf companion to TOI-4399 (HIP 94235), which hosts a mini-Neptune with an orbital period of 7.1 days. Their results show that the companion has a semi-major axis of ~ 60 AU and an inclination of $\sim 67.8^\circ$, indicating a modest misalignment between the companions and the transiting planet. Furthermore, previous studies have identified that the Hipparcos and Gaia proper motion anomalies of TOI-144 (π Men, Xuan & Wyatt 2020; De Rosa et al. 2020; Damasso et al. 2020), TOI-1144 (HAPT-11, Xuan & Wyatt 2020) and TOI-1339 (HD 191939, Lubin et al. 2022) are from giant planets at a few AU. By combining the proper motion anomalies and RVs, these studies obtained a constraint on the semi-major axis, orbital inclination and mass of the giant planets.

Among the sample of 66 targets with high proper motion anomalies, 33 systems have confirmed companions from previous surveys using AO/speckle imaging, mostly at separations from $0.1''$ to $2''$. We list the companion separations in Table 1 from published papers (Mason et al. 2001; Kraus et al. 2016; Ziegler et al. 2020, 2021; Winters et al. 2019; Howell et al. 2021; Lester et al. 2021) and TESS Follow-up Observing Program (TFOP). Additional AO imaging using Keck/NIRC2 and Subaru/SCEXAO will be presented in a follow-up paper.

Table 1. TOI/KOI/K2 with significant proper motion anomalies

Name	HIP Number	P_{pl} days	Exoplanet Archive Disposition	This work Disposition	Δv_G $m s^{-1}$	SNR_G	RUWE	distance ^d pc	comp. sep. ^e arcsec
TOI 1684	20334	1.16	PC	PC	4176.05	226.52	1.58	87.11	—
TOI 510	33681	1.35	APC	PC	2700.32	116.11	2.43	92.84	5.5 ⁵
TOI 394	15053	0.39	APC	EB	6995.08	94.97	3.18	141.7	3.22 ¹
TOI 6260	45961	2.39	PC	PC	6370.56	93.02	4.5	115.75	—

Name	HIP Number	P_{pl} days	Exoplanet Archive Disposition	This work Disposition	Δv_{Gaia} $m s^{-1}$	SNR _G	RUWE	distance pc	comp. sep. ^d arcsec
TOI 271	21952	2.48	APC	PC	8067.66	79.79	8.47	99.93	0.146 ²
TOI 1124	98516	3.52	APC	EB	6904.05	53.18	11.77	80.17	—
TOI 896	28122	3.53	FA	FA	3091.52	45.59	1.4	155.53	0.062 ²
TOI 5811	102295	6.25	PC	PC	2749.69	34.99	1.84	167.79	—
TOI 1418	83168	0.68	FA	SV	812.81	30.36	0.92	159.34	—
TOI 953	21000	2.97	FP	EB	6963.46	30.07	0.93	202.99	4.42 ¹
TOI 4314	22084	73.58	FA	SV	1370.99	29.95	2.23	153.05	—
TOI 680	58234	0.43	APC	PC	1590.25	29.68	3.71	160.05	0.78 ¹
TOI 2118	79105	2.34	FP	NEB	2493.51	27.9	4.37	188.03	—
TOI 6246	117249	6.78	PC	PC	832.73	26.3	1.07	188.45	-
TOI 1204	55069	1.38	PC	PC	418.69	23.51	0.98	106.45	0.375 ²
TOI 402 ^a	11433	4.76	CP	CP	187.62	22.46	0.89	44.86	1.44 ¹
TOI 402 ^a	11433	17.18	CP	CP	187.62	22.46	0.89	44.86	1.44 ¹
TOI 1946	70833	10.85	FP	NEB	3949.15	18.81	5.88	250.89	—
TOI 930	16881	4.9	PC	PC	1673.63	17.24	1.43	294.7	0.69 ¹
TOI 455 ^a (LTT 1445)	14101	3.12	CP	CP	354.41	14.1	1.07	6.86	A-BC 7.02 ⁴
TOI 455 ^a (LTT 1445)	14101	5.36	CP	CP	354.41	14.1	1.07	6.86	A-BC 7.02 ⁴
TOI 4568	77921	14.01	PC	PC	309.25	13.4	6.3	48.29	—
TOI 1665	27844	1.76	FP	NEB	126.38	13.17	0.94	66.44	1.9 ⁵
TOI 1837	67650	5.82	APC	EB	1145.74	12.85	7.37	152.67	0.15 ³
TOI 2666 ^b	45621	—	APC	EB	88.15	12.83	1.46	32.28	—
TOI 179	13754	4.14	PC	PC	72.24	12.06	0.99	38.63	—
TOI 1099	108162	6.44	PC	PC	51.94	11.16	1.16	23.64	7.64 ¹
TOI 5521	57386	18.51	PC	PC	420.92	10.78	1.68	136.95	0.6 ⁵
TOI 1719	44289	2.75	PC	PC	1864.24	8.31	10.38	236.54	0.12 ²
TOI 1151 (KELT-20)	96618	3.47	CP	CP	177.61	7.76	0.95	136.98	—
TOI 144 ^a (π Men)	26394	6.27	CP	CP	54.31	7.66	0.81	18.29	GP ⁶
TOI 144 ^a (π Men)	26394	124.46	CP	CP	54.31	7.66	0.81	18.29	GP ⁶
TOI 4399	94235	7.71	CP	CP	66.96	7.4	1.07	58.55	0.60 ⁸
TOI 4175	64573	2.16	PC	PC	131.36	7.18	1.34	46.32	1.67 ¹
TOI 2299	93711	165.02	PC	PC	74.33	6.87	1.06	34.27	—
TOI 1144 (HAPT-11)	97657	4.89	KP	CP	42.03	6.52	0.95	37.84	GP ⁶
TOI 201 ^a	27515	5.85	PC	PC	133.84	6.28	1.1	112.18	—
TOI 201 ^a	27515	52.98	CP	CP	133.84	6.28	1.1	112.18	—
TOI 635	47990	0.49	FA	PC	85.89	6.22	1.03	59.04	1.77 ¹
TOI 1831	65205	0.56	PC	PC	179.31	6.08	0.96	126.45	0.65 ³
TOI 1131	81087	0.59	PC	PC	1835.93	6.06	12.51	247.64	0.11 ²
TOI 4603	26250	7.25	CP	CP	307.19	5.92	1.0	224.15	—
TOI 909	82032	3.9	FP	NEB	42.47	5.81	1.04	51.65	1.35 ¹
TOI 575	41849	19.37	FP	EB	161.45	4.96	1.02	178.49	0.63 ¹
TOI 141	111553	1.01	CP	CP	37.88	4.92	1.09	47.77	0.44/1.20 ¹
TOI 128	24718	4.94	PC	PC	63.49	4.8	0.94	68.23	2.22 ¹
TOI 2017	74685	5.5	FP	EB	278.86	4.37	7.12	98.57	—
TOI 6265	49508	5.79	PC	PC	88.11	4.15	1.09	71.29	-
TOI 5140	42403	15.61	PC	PC	24.67	3.85	0.98	35.24	—
TOI 5962	112486	1.92	PC	PC	147.97	3.80	0.97	127.27	—
TOI 230	114003	13.34	FA	PC	106.85	3.78	1.01	141.62	—
TOI 5383	69275	2.8	PC	PC	120.17	3.73	2.53	102.09	—

Name	HIP Number	P_{pl} days	Exoplanet Archive Disposition	This work Disposition	Δv_{Gaia} $m s^{-1}$	SNR _G	RUWE	distance pc	comp. sep. ^d arcsec
TOI 1339 ^a	99175	8.88	CP	CP	32.34	3.73	1.05	53.49	GP ⁶
TOI 1339 ^a	99175	28.58	CP	CP	32.34	3.73	1.05	53.49	GP ⁶
TOI 1339 ^a	99175	38.35	CP	CP	32.34	3.73	1.05	53.49	GP ⁶
TOI 1339 ^a	99175	101.12	CP	CP	32.34	3.73	1.05	53.49	GP ⁶
TOI 1339 ^a	99175	284	CP	CP	32.34	3.73	1.05	53.49	GP ⁶
TOI 621	44094	3.11	APC	PC	97.46	3.69	0.84	182.31	2.06 ¹
TOI 5079	24007	1.49	FP	PC	99.1	3.47	0.98	76.93	2.7 ⁵
TOI 1271	66192	6.13	KP	CP	53.15	3.47	0.96	92.04	—
TOI 222 ^b	118045	—	FP	EB	66.43	3.46	1.78	85.42	—
TOI 522	40694	0.4	PC	PC	110.24	3.36	0.99	111.73	0.75 ¹
TOI 1730 ^a	34730	2.16	PC	CP	52.09	3.32	1.14	35.65	—
TOI 1730 ^a	34730	6.23	PC	CP	52.09	3.32	1.14	35.65	—
TOI 1730 ^a	34730	12.56	PC	CP	52.09	3.32	1.14	35.65	—
TOI 1799	54491	7.09	PC	PC	40.65	3.31	1.03	62.23	—
TOI 369	115594	5.46	PC	PC	276.13	3.21	1.36	227.75	0.69 ¹
TOI 906	78301	1.66	PC	PC	104.0	3.04	0.92	135.41	1.35 ¹
K03158 ^a (Kepler444)	94931	3.60	CP	CP	256.64	45.44	0.99	36.55	1.84 ⁷
K03158 ^a (Kepler444)	94931	4.55	CP	CP	256.64	45.44	0.99	36.55	1.84 ⁷
K03158 ^a (Kepler444)	94931	6.18	CP	CP	256.64	45.44	0.99	36.55	1.84 ⁷
K03158 ^a (Kepler444)	94931	7.74	CP	CP	256.64	45.44	0.99	36.55	1.84 ⁷
K03158 ^a (Kepler444)	94931	9.94	CP	CP	256.64	45.44	0.99	36.55	1.84 ⁷
K06139	94780	0.91	FP	EB	424.76	7.3	1.9	237.73	—
K01924	96501	2.12	FP	EB	1003.70	4.32	12	106.51	—
K06364	93954	1.54	FP	EB	117.26	3.29	1.58	139.6	—
EPIC204165788	80474	0.75	FP	EB	2264.77	47.42	2.7	123.2	—
EPIC201488365	54766	3.36	PC	EB	592.84	19.27	0.96	146.39	—
EPIC212096658	41431	1.47	PC	EB	550.58	10.96	10	49.43	—
EPIC204506777	78977	1.63	FP	EB	204.61	3.25	3.29	150.92	—

^aMultiple planet systems.

^bSingle transit planet candidate, no orbital period.

^cThe flags come from NASA Exoplanet Archive. CP: Confirmed Planet, PC: Planet Candidate, APC: Ambiguous Planet Candidate, FP: False Positive, FA: False Alarm.

^dDistances are from Gaia DR3 release (Gaia Collaboration et al. 2022)

^eCompanion separation from published papers or TFOP. The references are: 1. Ziegler et al. (2020, 2021); 2. Lester et al. (2021); 3. TFOP, observation using Palomar/PHARO (PI: D. Ciardi); 4. Rodriguez et al. (2015); Winters et al. (2019); 5. WDS catalog (Mason et al. 2001); 6. GP: the proper motion anomalies of TOI144, TOI1144 and TOI1339 are from giant planets (Xuan & Wyatt 2020; De Rosa et al. 2020; Damasso et al. 2020; Lubin et al. 2022); 7. Dupuy et al. (2016); Zhang et al. (2022). 8. Zhou et al. (2022)

4. STATISTICAL ANALYSIS OF TOIS

4.1. Planet candidates vs. False positives

We first analyzed the fraction of false positives of the transiting detections in the sample. Table 1 lists the NASA Exoplanet Archive dispositions that classify TOIs/KOIs/K2 candidates, including Confirmed/Known Planet (CP/KP), Planet Candidate (PC), Ambiguous Planetary Candidate (APC), False Positive (FP), and False Alarm (FA). We also present different reasons for the false positive/false alarm dispositions in Table 1. A false positive or false alarm flag is assigned in several situations. The first scenario is *Eclipsing Binaries* (EBs), in which the secondary stars graze the edge of primaries, and the reduction in brightness is indistinguishable from transits of smaller planets. The second scenario is the contamination by a *Nearby Eclipsing Binary* (NEB) as multiple stars are unresolved due to the large pixel scale of *Kepler* and *TESS* (4'' for *Kepler* and 21'' for *TESS*). In this case, the bright primary star dilutes the light of a nearby, dimmer, eclipsing binary pair to the point at which the eclipses seem as

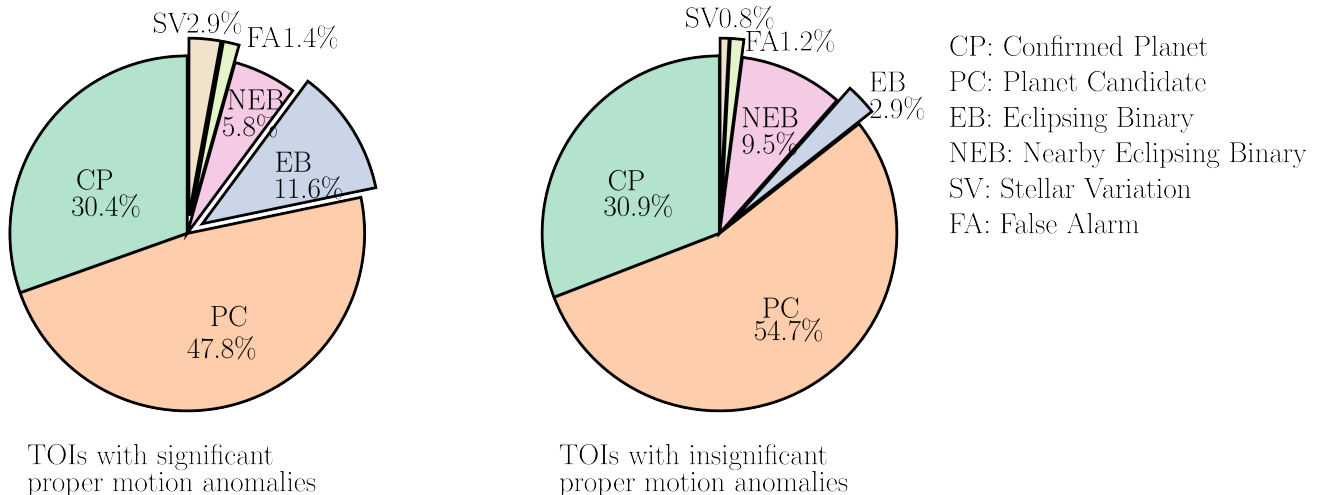


Figure 3. Right panel: the fraction of confirmed planets, planet candidates, and several false positives of TOIs in our high SNR sample. Left panel: the fraction of the same categories but for low SNR TOIs. The two samples are both limited to 300 pc. We only present TOIs in this figure because the majority of KOI/K2 targets in our sample are EBs.

shallow as a planetary transit. In addition, stellar variation (SV) and spacecraft systematics errors (SSE) can also mimic the dips in light curves similar to those from transiting planets.

To break down the FP into the EB/NEB/SV flag, we refer to the TESS Follow-Up Observing Program Sub-Group 1&2 (TFOP SG1 & SG2) disposition and notes as a guide for TOIs. TFOP SG1 performs seeing-limited imaging of the TOIs using ground-based telescopes with higher spatial resolution to check whether the transits occur on target. They detected four TOIs (TOI-2118, TOI-1665, TOI-909, TOI-1946) in our sample as NEB. In addition, TFOP SG2 identified 8 EBs based on odd-even transit difference (TOI-394, TOI-1124, TOI-575,) or RVs from TRES+FIRES (TOI-953, TOI-1837, TOI-2017, TOI-2666, TOI-222). In our sample, the majority of KOIs and K2 transiting signal are from EBs based on the results from Kepler/K2 EB catalogs (Slawson et al. 2011; Armstrong et al. 2015; Rizzuto et al. 2017; Kruse et al. 2019). We present the details of each FP in our sample in Appendix A.

The left panel in Figure 3 presents the fraction of confirmed planets, planet candidates, eclipsing binaries, nearby eclipsing binaries, and other false positives in TOIs with significant proper motion anomalies (58 TOIs). We have chosen to only present the results of TOIs for a homogeneous comparison, because follow-up observations for candidates of TOI, KOI, and K2 are conducted through various projects, and the majority of KOIs and K2 targets in our sample are eclipsing binaries (EBs). For comparison, we show a control sample from TOIs with $\text{SNR}_G < 3$ and distances smaller than 300 pc (254 TOIs). We also break down the false positives in

the HGCA-low-SNR sample into the same categories as our targets based on the TFOP SG1 disposition. The HGCA-high-SNR TOIs contain a higher fraction of false positives (up to 21.8% compared to the 14.4% of HGCA-low-SNRs TOIs). The difference is mainly from the excess of EBs among the HGCA-high-SNR TOIs, taking up $\sim 11.6\%$ of the sample. The EB false positives result from contamination of triple systems with close-in eclipsing binaries. Due to the dilution of light curves by multiple sources in the same pixel, the transit depth appears comparable to planetary transits around single stars. Our finding agrees with previous studies. Ziegler et al. (2020) presents that hot Jupiters are more common in binaries with wide companions compared to field stars. But Ziegler et al. (2021) argues that these findings can be attributed to false positive contamination arising from tertiary companions to closely orbiting eclipsing binaries. In contrast, other false positives, including NEB, stellar variability, and spacecraft false alarms, account for a similar share in the two samples.

4.2. Orbital period of TOIs with significant proper motion anomalies

In this section, we compare the orbital periods of planets around TOIs with significant Hipparcos-Gaia astrometric acceleration and those with marginal astrometric acceleration. Figure 4a presents the planet orbital periods and the Gaia differential velocities of TOIs with high-SNR and low-SNR proper motion anomalies, respectively. The Gaia differential velocities are defined in Section 2 (see Eqn. 3) We exclude systems with false positive and false alarm dispositions. We do not include the eight KOIs and K2 targets because seven of

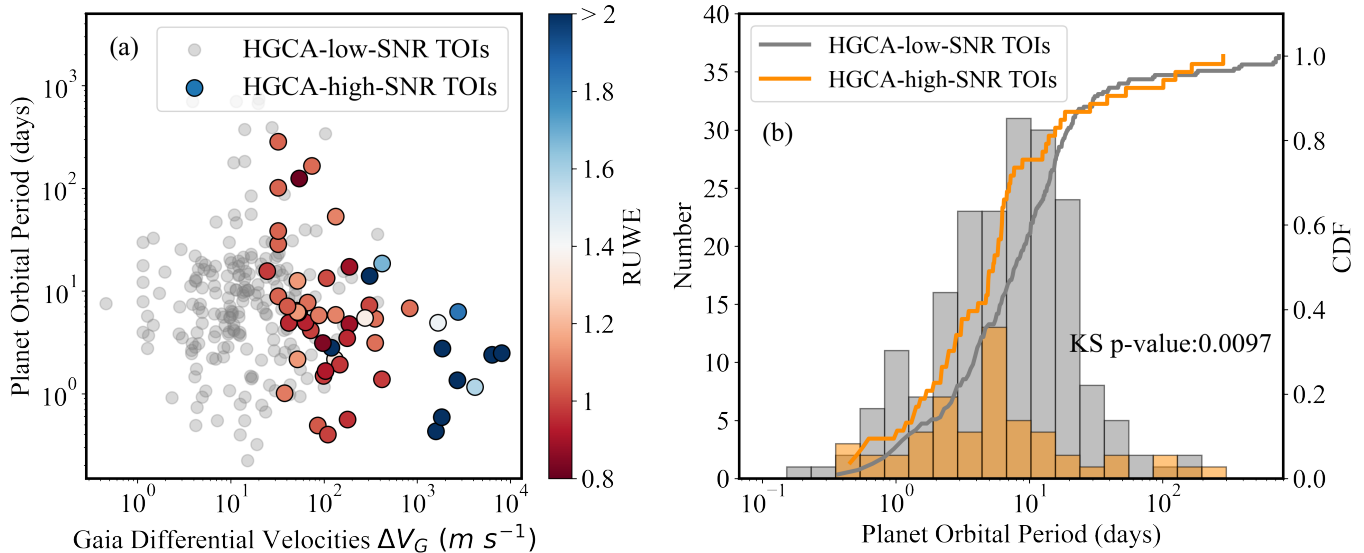


Figure 4. Panel a: planet orbital period vs. differential velocities at Gaia epoch of TOIs with significant proper motion anomalies (color-coded by their Gaia DR3 RUWE) and TOIs with marginal proper motion anomalies (grey). We exclude TOIs with FP/FA dispositions. High-SNR TOIs with $\text{RUWE} \geq 1.4$ are in red, whereas those with $\text{RUWE} < 1.4$ are in blue. Panel b: marginalized distribution of planet orbital periods of high (orange) and low (grey) SNR TOIs overlapped with the cumulative distribution function. We exclude TOIs with FP/FA dispositions.

them are false positives. We colored HGCA-high-SNR TOIs by their Gaia DR3 Renormalised Unit Weight Error (RUWE). A RUWE value greater than 1.4 usually indicates that the source is non-single and the two components are too close to be fully resolved by Gaia (Lindgren et al. 2018).

The HGCA-high-SNR TOIs with high RUWE mostly have differential velocities beyond one thousand $m s^{-1}$, including TOI-271, TOI-680, TOI-930, TOI-1719, and TOI-1131. The high differential velocities are consistent with these TOIs having close stellar companions with separations below $1''$ (see Table 1)². In comparison, HGCA-high-SNR TOIs with low RUWE have differential velocities from dozens to a few hundred $m s^{-1}$. In some systems, the velocities in the middle range are from stellar companions at relatively wider separation. For instance, TOI-402, TOI-4175, TOI-635, TOI-128 are all in this regime and have companions with separations $> 1''$. In other cases, low-mass companions, such as brown dwarf companions and giant planets, cause the primaries to orbit around the barycenter at velocities from dozens to a few hundred $m s^{-1}$. Their low RUWE indicates that the single-star model is still a good fit because the substellar companions are much fainter than primaries. In our sample, the Hipparcos-Gaia proper

motion anomalies reveal the existence of giant planets at a few au in TOI-144(π Men), TOI-1144(HAPT-11), and TOI-1339 systems.

Figure 4a shows a tentative inverse correlation between the orbital period of transiting planets and the Gaia differential velocities of their host stars. The planet periods of TOIs with differential velocities $> 1000 m s^{-1}$ are all shorter than ten days. Figure 4b displays the distributions of planet orbital periods of HGCA-high-SNR and HGCA-low-SNR TOIs. We include 53 HGCA-high-SNR TOIs and 200 HGCA-low-SNR TOIs. We can see that orbital periods of transiting planets in HGCA-high-SNR TOIs are generally shorter than in HGCA-low-SNR TOIs. A Kolmogorov-Smirnov test shows that the difference between two samples' planet orbital period distributions is statistically significant ($p\text{-value} = 9.7 \times 10^{-3}$).

To explore whether the trend found in Figure 4 hold true for a larger sample, we compare the orbital periods of planets in binary and single TOIs/KOIs from Kraus et al. (2016); Ziegler et al. (2020, 2021); Howell et al. (2021); Lester et al. (2021). Figure 5a presents the stellar companion separations and planet orbital periods of these TOIs and KOIs. In Figure 5b, We include 265 and 56 confirmed planets in binary and single TOIs from Ziegler et al. (2020, 2021); Howell et al. (2021); Lester et al. (2021). In Figure 5c, we include 138 and 296 confirmed planets in binary and single KOIs from Kraus et al. (2016). To rule out the influence of EBs that usually have short periods, we only select confirmed planets (CP) or known planets (KP) from their sample. We also

² Except for TOI-510 which has a companion at $5.5''$ reported from WDS catalog. The Hipparcos Gaia acceleration indicates there might be another unresolved companion at a closer separation.

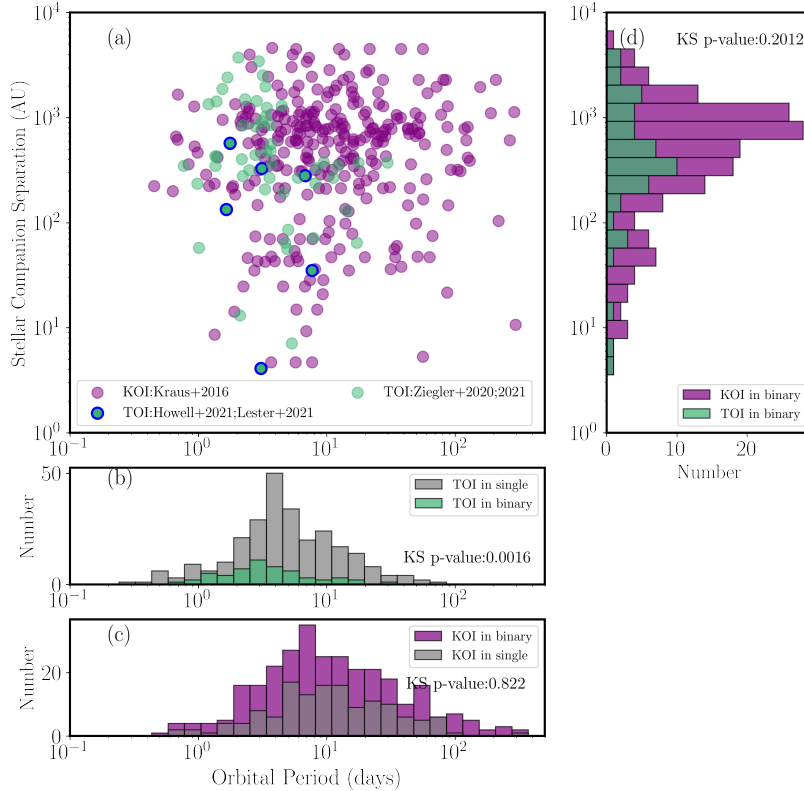


Figure 5. Panel a: planet orbital period vs. stellar companion separations of TOIs (green, Ziegler et al. 2020, 2021; Lester et al. 2021; Howell et al. 2021) and KOIs (purple, Kraus et al. 2016) in binary systems. We only include confirmed planets (CP) or known planets (KP). Panel b: marginalized distribution of planet orbital periods of TOIs in binaries (green) and singles (grey). Panel c: same as panel b but for KOIs in binary (purple) and single (grey) systems. Panel d: marginalized distribution of stellar companion separations of TOIs (green) and KOIs (purple) in binaries.

removed duplicate TOIs resulting from the overlap between different surveys. We did not apply a distance cutoff to their sample, as such an approach would have resulted in a further decrease in the size of the sample. But most of their targets are within 400 pc, with a small fraction extending beyond 800 pc (See Figure 1 in Kraus et al. 2016 and Ziegler et al. 2021). We find that TOIs in binaries have orbital periods statistically shorter than those in single systems (p-value = 0.0016). However, we do not see a significant difference between confirmed Kepler planets in binaries and singles (p-value=0.82).

A few possibilities can explain the different results in the TOI and KOI samples. First, the difference in sensitivity between the two missions may explain the observed disparity, as *TESS* detected more short-period planets within ten days but fewer at longer periods than *Kepler*. However, this explanation alone cannot account for the shorter orbital periods of planets in binary TOIs, since *TESS* searches for planets without considering the binarity of the targets. The second possibility is that stellar companions in KOI sample have relatively larger separations as they are generally more distant and fainter than TOIs. Therefore, companions in KOI sam-

ple are less influential in shaping the planets’ orbital periods. Ziegler et al. (2020, 2021) and Kraus et al. (2016) both present stellar companions to KOIs/TOIs at separation from a few AU to a few thousand AU. However, Figure 5d illustrates that the distributions of stellar companion separations in the TOI and KOI samples do not exhibit a significant difference (p-value=0.20). Thirdly, the difference between binary and single TOIs might potentially be attributed to the relatively small size of TOIs in binary systems. Therefore, a larger sample of TOIs in binaries is required to reach a more decisive conclusion. Finally, the disparity in planet periods observed between the TOI and KOI samples may be due to the fact that *Kepler* has higher precision and is thus more sensitive to smaller planets than *TESS*. Consequently, the two missions may be observing different populations of planets. To test the hypothesis, we need to revise the radii of planets orbiting TOIs/KOIs in binary systems by accounting for the flux dilution.

In short, the reason why the *TESS* bias affects binary and single systems differently is not yet understood, and a larger sample of TOIs is needed to draw a more definitive conclusion. If the TOIs in binaries do have shorter

orbital periods (<10 days), they might form in truncated disks by the companions. Besides, planets' survival probability is likely higher at close-in orbits because the host stars provide more shield to resist the gravitational disturbance from the companions.

4.3. Differential velocity distribution of TOIs vs. field stars

As detailed in section 2, the differential velocities can be approximately seen as the projected orbital velocities of the primary stars around the system barycenter, which increases with the companion masses and decreases with orbital distances. In this section, we compare the Gaia differential velocities of HGCA-high-SNR TOIs with field stars, which consists of all stars exhibiting significant proper motion anomalies from HGCA within 300 pc. Figure 6 presents the results. The differential velocities of field stars exhibit a peak around $3000 m s^{-1}$ and a broader bump centered at $\sim 200 m s^{-1}$ to the left. The velocity magnitude at the peak is consistent with differential velocities caused by stellar companions with orbital periods from a few years to a few hundred years (sensitive range for Hipparcos-Gaia proper motion anomalies method). For example, a solar mass star would have a differential velocity of around $4400 m s^{-1}$ with a $0.5 M_{\odot}$ companion at an orbital period of approximately 25 years, assuming a face-on orbit. As the orbital periods increase or companion masses decrease, the stellar companions' velocities produce a tail at lower velocities. For example, a $0.01 M_{\odot}$ companion would cause a velocity of around $100 m s^{-1}$ for a solar mass star at 25 years period.

Compared to field stars, the distribution of HGCA-high-SNR TOIs displays a higher peak at velocities around $100 m s^{-1}$ with a shortfall at high differential velocities. These distributions suggest that transiting planets are more likely to form in binaries when the companions have lower masses or are at wider separations. Our results are compatible with the previous studies that planets are less common in close binary systems compared to single systems or wide binaries (Wang et al. 2015; Kraus et al. 2016; Ziegler et al. 2020, 2021; Hirsch et al. 2021; Moe & Kratter 2021). In a recent study, Moe & Kratter (2021) finds that the occurrence rate of planets in binaries with $a < 10$ AU is roughly 15% of that in single systems, while wide binaries with $a > 200$ AU have similar planet occurrence rates as single stars. The recent ALMA high-resolution surveys also find that disks in multiple systems are smaller, fainter, and less long-lived than those in singles (Cox et al. 2017; Akeson et al. 2019; Manara et al. 2019; Zurlo et al. 2020; Zagaria et al. 2023). These findings support the theory

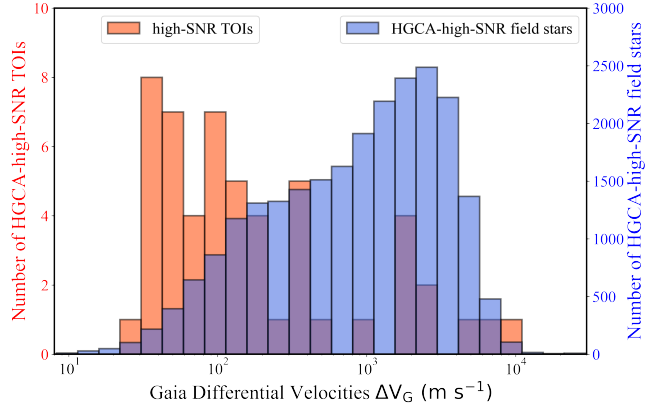


Figure 6. Gaia differential velocity distribution of TOIs with significant proper motion anomalies (red) compared to field stars (blue). The field star sample consists of all stars with significant proper motion anomalies from HGCA within 300 pc. The differential velocity are in log scale. We exclude TOIs with FP/FA disposition.

that close companions tidally truncate the circumstellar discs and reduce the reservoir of material available to assemble planetary embryos (Paczynski 1977; Rudak & Paczynski 1981; Jang-Condell et al. 2015; Pichardo et al. 2005; Zagaria et al. 2023).

5. ORBIT CHARACTERIZATION OF BENCHMARK SYSTEM: LTT 1445 ABC

In the section, we present the results of proof-of-concept system LTT 145 ABC, for which we characterize the three dimensional orbits of the companion pair BC around A with RVs, Hipparcos-Gaia astrometric acceleration and relative astrometry from AO imaging.

5.1. Background

LTT 1445 ABC (TOI-455) is the closest M dwarf triple known to harbor multiple planets at a distance of 6.86 pc (Rossiter 1955; Luyten 1957, 1980; Winters et al. 2019, 2022). The hierarchical system consists of a primary LTT 1445 A ($0.268 R_{\odot}$, $0.257 M_{\odot}$) orbited by a M dwarf pair BC at a separation of $\sim 7''$ (Dieterich et al. 2012; Rodriguez et al. 2015). LTT 1445 A has two transiting super-Earths and one non-transiting planet: LTT 1445 Ab ($P_b = 5.36$ days, $r_b = 1.3 R_{\oplus}$, $m_b = 2.87 \pm 0.25 M_{\oplus}$), LTT 1445 Ac ($P_c = 3.12$ days, $r_c < 1.15 R_{\oplus}$, $m_c = 1.54 \pm 0.2 M_{\oplus}$), LTT 1445 Ad ($P_d = 24.3$ days, $m_d = 2.72 \pm 0.25 M_{\oplus}$) (Winters et al. 2019, 2022; Lavie et al. 2022). The BC subsystem is a visual binary pair with a separation of $\sim 1''$. Using archival astrometry from Fourth Interferometric Catalog (FIC) and Differential Speckle Survey Instrument (DSSI), Winters et al. (2019) found that LTT 1445 C orbits around B in an eccentric and edge-on orbit with a period

Table 2. LTT 1445A RVs

Time (BJD - 2450000)	RV (m/s)	σ_{RV} (m/s)	Inst
9482.1	1.69	1.37	HIRES
9587.81	-1.54	1.37	HIRES
9824.13	2.33	1.29	HIRES
9832.03	3.5	1.46	HIRES
9947.73	0.45	1.2	HIRES

NOTE—Times are in BJD - 2450000.0. The RV uncertainties do not include RV jitter. We present 5 unpublished HIRES RVs in this table. All RV data utilized in the orbit fitting, including those sourced from the literature, are available in a machine-readable format.

of ~ 36 years ($e_{C,B} = 0.5 \pm 0.11$, $i_{C,B} = 89^\circ.64 \pm 0.13$, $a_{C,B} = 8.1 \pm 0.5\text{AU}$, $\Omega_C = 137.63^\circ \pm 0.19$). However, it is unclear how the companion pair orbit around the primary. Therefore, we utilized the Hipparcos-Gaia proper motion anomalies, combined with primary RVs and relative astrometry to characterize the orbit of LTT1445 BC pair around the primary A. Furthermore, we constrain the mutual inclination between orbital plane of C around B and that of the subsystems around the primary. LTT 1445 A is targeted by James Webb Space Telescope Cycle 1 GO Program 2708 (PI Z. Berta Thompson) to investigate the presence of an atmosphere of the planet b. Our characterization of the companion pair’s orbit provides context for the dynamical stability of the system.

5.2. Orbit Fitting

We use 9 archival RVs of LTT1445 A taken with HARPS between 2004 and 2013 from [Trifonov et al. \(2020\)](#) and 136 published RVs from 2019 to 2021 taken with 5 high-precision spectrographs including the W. M. Keck Observatory echelle spectrograph HIRES, ESPRESSO, HARPS, MAROON-X and PFS from [Winters et al. \(2022\)](#). We also include 5 RVs we newly collected between Sep. 2021 and Jan. 2023 using HIRES (see Table 2). The proper motion anomalies of LTT 1445 A at Hipparcos and Gaia epoch are from HGCA. Finally, we adopt two published relative astrometric measurements taken at 2003 and 2010 from [Dieterich et al. \(2012\)](#) and [Rodriguez et al. \(2015\)](#) (see Table 3). We consider BC pair as one object and use the relative astrometry of mass center of BC subsystem to primary A.

Table 3. Relative Astrometry used in the Orbit Characterization for LTT 1445BC around A

Date		θ ($^\circ$)	ρ ($''$)	Instrument	Reference
2003.4620	A-B	315.0	7.706	HST/NICMOS	1
2003.4620	B-C	138.1	1.344	HST/NICMOS	1
2003.4620	A - BC ¹	314.74	7.13	HST/NICMOS	3
2010.594	A-B	313.79 ²	7.20	Lick/IRCAL	2
2010.594	B-C	138.41	0.41	Lick/IRCAL	2
2010.594	A-BC	314.91	7.02	Lick/IRCAL	3

¹ Relative astrometry of the mass center of BC from A.

² Quadrant ambiguous; the position angle here has been changed by 180 degrees relative to the original result.

References— (1) [Dieterich et al. \(2012\)](#); (2) [Rodriguez et al. \(2015\)](#); (3) Derived in this work.

We use open source package *orvara* ([Brandt et al. 2021](#)), which performs a parallel-tempering Markov Chain Monte Carlo (MCMC) fitting. In total, our analysis uses 15 free parameters. Two of them are the masses of the host star (M_A) and combined mass of companion pair (M_{BC}). Six orbital parameters define the orbit of companion pair, including semi-major axis (a), inclination (i), longitude of the ascending node (Ω), mean longitude at a reference epoch (t_{ref}) of 2455197.5 JD (λ_{ref}), and the eccentricity (e) and the argument of periastron (ω) in the form of $e \sin \omega$ and $e \cos \omega$. We also included six parameters to fit the zero-point for RV data from different instruments. As there was a fiber exchange for HARPS in 2015, we use different RV zero points for HARPS RVs taken before and after 2015. The last parameter is the intrinsic jitter of RV data. We ignore the transiting planets because their RVs amplitudes are expected to be smaller than the stellar jitter. The proper motion anomalies from inner planets are also nearly zero because signals cancel out when the orbital periods are much shorter than the observing window duration of *Hipparcos* and *Gaia*. We use the primary mass and companion masses from [Winters et al. \(2019\)](#) as priors in our fitting and bound the jitter between 0 to 10 m s^{-1} . The likelihood is calculated by comparing the measured separations, position angles, absolute astrometry, and radial velocities to those of a synthetic orbit and assuming Gaussian errors ([Brandt et al. 2021](#)).

We use 100 walkers to sample our model and the chains converge after 2.5×10^5 steps. We discarded the first 30% as burn-in portion. Figure 7 shows the best-fit orbit (black lines) from our MCMC chains, including fitted astrometric orbit, RVs and Hipparcos-

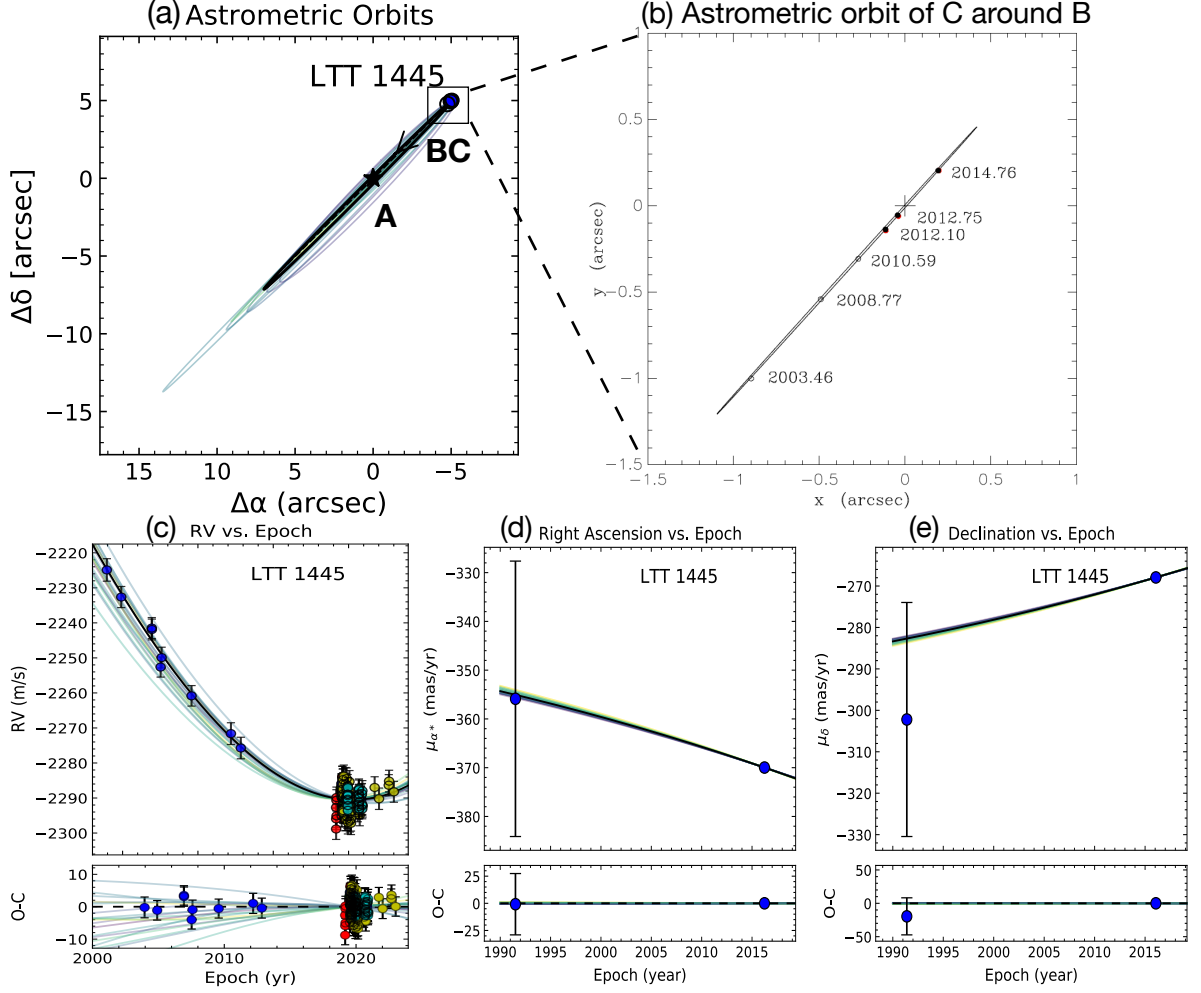


Figure 7. Orbit characterization of LTT 1445 BC mass center around A using RVs, relative astrometry and absolute astrometry from Hipparcos and Gaia. (a): relative astrometry orbits of LTT 1445 BC pair around A. The blue filled circles are two observed relative astrometry used in our analysis. (c): Observed and fitted RVs of LTT 1445 from HARPS, HIRES, ESPRESSO, MAROON-X, PFS. (d)-(e): Observed and fitted Hipparcos and Gaia proper motion of LTT 1445 A in right ascension and declination. In all of above panels, the thicker black lines represent the best-fit orbit in the MCMC chain while the other 50 lines represent random draws from the chain; (b): relative astrometry orbits of LTT 1445 C around B from [Winters et al. \(2019\)](#).

Gaia proper motions. The reduced χ^2 of RVs indicates a good fit and accurate measurement errors, with values of 0.97. We obtain a dynamical mass of $M_A = 0.251^{+0.010}_{-0.010} M_\odot$ for primary A and mass of $M_{BC} = 0.39^{+0.009}_{-0.009} M_\odot$ for BC subsystem, which agree with published values from [Winters et al. \(2022\)](#) within 1σ . Our best-fit model shows that the subsystem BC orbits around primary A in an eccentric and edge-on orbit ($a_{BC,A} = 58^{+20}_{-16}$ AU, $e_{BC,A} = 0.375^{+0.037}_{-0.064}$, $i_{BC,A} = 88^{+1.3}_{-1.4}$, $\Omega_{BC,A} = 135.15^\circ \pm 0.28$, see Table 4 for other parameters). We compute the mutual inclination Δi between orbital plane of BC around A and that of C around B with their inclination ($i_{C,B}$, $i_{BC,A}$) and

longitude of ascending node ($\Omega_{C,B}$, $\Omega_{BC,A}$):

$$\cos \Delta i = \cos i_{C,B} \cos i_{BC,A} + \sin i_{C,B} \sin i_{BC,A} \cos(\Omega_{C,B} - \Omega_{BC,A}) \quad (4)$$

We obtained the mutual inclination $\Delta i = 2^\circ.88 \pm 0.63$. Therefore, LTT 1445 ABC is a flat system where the subsystem BC orbits around A in nearly the same plane as their orbit around each other. Because the LTT 1445 A is a slow rotator ($P_{tot} \sim 84$ days, [Winters et al. 2019](#)), we are not able to measure the spin-orbit angle of two transiting planets b and c relative to the primary through Rossiter-MacLaughlin effect. However, the probability of observing the two transiting planets and companion pair BC all have edge-on orbits is notably low, if we assume their orbits are independent. Specifically, if the $\cos(i)$ values of planet b, c, and companion

pair BC are drawn randomly from a uniform distribution between 0 and 1, the probability of observing all these bodies to have inclinations within the range of 87° to 90° is only 0.014%. Therefore, it is highly likely that the transiting planet orbits are coplanar with the orbit of the BC companions. Meanwhile, the alignment of the non-transiting planet LTT 1445 Ad with the inner planets is subject to significant uncertainty. Located at a distance of 0.09 AU, the angle range for a transiting configuration is only 1.6° . A plausible scenario is that LTT 1445 Ad is aligned with the inner planets but is located outside the transiting configuration. A detailed dynamical study might yield interesting constraints on the possible orbits of planet d, but is outside the scope of this paper.

5.3. Implication for planet formation

One piece that needs to be added to understand the effect of companions on planet formation is the inclination of the companion orbits. Inclination plays a vital role in the dynamic interaction between the companions and inner planets or the protoplanetary disks. For example, the Kozai-Lidov effect (Kozai 1962; Lidov 1962) occurs when the mutual inclination between two objects is greater than $\sim 40^\circ$, causing the inner objects to be unstable. Previous studies have also found that an inclined outer companions may misaligned the orbit of inner planets (Huber et al. 2013; Zhang et al. 2021). Fortunately, the combination of Hipparcos and Gaia astrometry and RVs allow us to characterize the three-dimensional orbits of the companions. In this work, we present the results of triple system LTT 1445, in which LTT 1445 BC orbit around the primary A with a semi-major axis of ~ 58 AU. The LTT 1445 system bears a remarkable resemblance to the Kepler-444 triple system, where Kepler-444 BC orbits around A in an edge-on orbit and is likely to be aligned with the orbit of five transiting planets around the primary A (Dupuy et al. 2016; Zhang et al. 2022). LTT 1445 and Kepler-444 both agree with the statistical results reported by Dupuy et al. (2022), which concludes that low mutual inclinations between planets and companions are required to explain the observed orbital arcs in 45 binary systems containing *Kepler* planet candidates. One may ponder whether the coplanarity of the systems relates to the planet’s formation in a dynamically hostile environment.

Zanazzi & Lai (2018) investigated the evolution of disk inclinations in binary systems and found that effective realignment between the circumstellar disks around the primary star and companions tends to occur when the companions are closer than 200 AU. Considering that LTT1445 BC has a semi-major axis of ~ 58 AU, it is

plausible that the companions were initially misaligned with the primary disk but later underwent realignment during their evolution. Another close binary HIP94235 ($a \sim 50$ AU) is consistent with the possibility in which the primary hosts a transiting mini-Neptune. The companion HIP94235B exhibits an inclination of around 68° (Zhou et al. 2022), which suggests a minimum misalignment of 22° between the companions and the transiting planet. Given that HIP94235 is part of a young comoving group (~ 120 Myr, Zhou et al. 2022), it is possible that the realignment between the companion and the disk is still ongoing. Alternatively, it is also possible that the LTT 1445 BC were initially aligned with the primary disk from the onset. In this case, the fully con-planar configuration and close separation of LTT 1445 triples are consistent with the disk fragmentation scenario that gravitational instability in a shearing disk might produce multiples stars (Adams et al. 1989; Moe & Kratter 2018; Offner et al. 2022). In either possibility, although the companions likely truncated the primary’s circumstellar disk, there was still enough disk material remaining to form multiple planets. In short, constraining the mutual inclination between planets and stellar companions in more systems is needed to understand the mechanisms behind planet formation in close binary systems.

6. CONCLUSIONS

We have presented a study of transiting planets with systems that show significant Gaia-Hipparcos accelerations. Our conclusions are as follows:

1. We presented a catalog of 66 transiting planet hosts (58 TOIs, 4 KOIs, and 4 K2 planet candidates) within a 300 pc volume limit with significant *Hipparcos* and *Gaia* proper motion anomalies through cross-matching the TOI/KOI/K2 catalogs with HGCA. The parameters of these targets are presented in Table 1. Among these targets, 33 have directly imaged stellar companions, either from published papers or the ExFOP website.
2. For transiting planet candidates identified by *TESS*, we evaluated the reliability of the transits based on the radial velocities obtained with Keck/HIRES and the TESS Follow-Up Observing Program. We found that TOIs with high proper motion anomalies have nearly four times more eclipsing binary classifications than TOIs with insignificant proper motion anomalies. The excess of EBs in HGCA-high-SNR TOIs might be from the contamination of triple systems.

Table 4. MCMC Orbital Posteriors for LTT 1445

Parameter	Median $\pm 1\sigma$	Best-fit value
Stellar parameters		
Host-star mass M_A (M_\odot)	0.25 ± 0.01	0.25
Companion pair mass M_{BC} (M_\odot)	0.39 ± 0.09	0.39
Orbital parameters		
Semi-major axis a (AU)	58^{+16}_{-10}	63.45
Orbital period P (yr)	549^{+243}_{-136}	629.54
Inclination i (deg)	$88.5^{+1.3}_{-1.3}$	88.82
$\sqrt{e} \sin \omega$	$-0.568^{+0.036}_{-0.025}$	-0.24
$\sqrt{e} \cos \omega$	$-0.14^{+0.28}_{-0.24}$	-0.58
Eccentricity e	$0.375^{+0.084}_{-0.037}$	0.4
Mean longitude at $t_{\text{ref}} = 2455197.5$ JD, λ_{ref} (deg)	210.3 ± -2.1	211.19
Longitude of the ascending node Ω (deg)	135.15 ± 0.28	135.10
Parallax (mas)	$145.6923^{+0.0040}_{-0.0040}$	145.69
Argument of periastron ω (deg)	256^{+28}_{-21}	247.52
Time of periastron $T_0 = t_{\text{ref}} - P \frac{\lambda - \omega}{360}$ (JD)	2480796^{+5304}_{-5663}	2478401.65
Other Parameters		
RV jitter σ (m s^{-1})	$2.74^{+0.21}_{-0.18}$	2.73
HARPS pre-2015 RV zero point (m s^{-1})	3225.67^{+166}_{-177}	3162.27
HARPS post-2015 RV zero point (m s^{-1})	-2188.44^{+166}_{-176}	-2250.74
EXPRESSO RV zero point (m s^{-1})	3232.41^{+166}_{-177}	3169.01
MAROON-X RV zero point (m s^{-1})	-2226.99^{+166}_{-177}	-2290.44
HIRES RV zero point (m s^{-1})	-2225.24^{+166}_{-177}	-2288.68
PSF RV zero point (m s^{-1})	-2226.55^{+166}_{-177}	-2289.98

NOTE—The χ^2 of relative astrometry is 0.09 for separations and 0.06 for PAs, with 2 measurements for each. The χ^2 of the Hipparcos and Gaia proper motion differences is 2.64 for four measurements. The χ^2 of RV is 146.80 for 150 measurements.

- We translated the proper motion anomalies into differential velocities between the epochs of Hipparcos and Gaia, expressed in units of m s^{-1} . We observe a tentative inverse correlation between transiting planet orbital periods and *Gaia* differential velocities, with short planet periods occurring preferentially with more massive and closer companions. Additionally, our findings suggest a possible trend of shorter planet periods in binaries, although this could be an artifact of the *TESS* observation bias. If the trend is genuine, it supports the theory that planets in binaries form in smaller protoplanetary disks truncated by their companions.
- We observe that HGCA-high-SNR TOIs exhibit lower differential velocities than the entire population of significant proper motion anomalies stars within 300 pc in HGCA catalog. This comparison

indicates that planets are more likely to persist in systems with low-mass companions or wider stellar companions.

- We determined the three-dimensional orbit of the companion pair BC around the primary star A in the triple system LTT 1445, which also hosts two transiting planets. Our analysis indicates that LTT 1445 is a flat system, with the orbital plane of BC around A being almost coplanar with the orbital plane of the outer planet c around B ($\Delta i \sim 2.88^\circ$). This coplanarity may account for the survival of multiple planets in an otherwise dynamically challenging environment.

Future observations will provide opportunities to confirm potential companions in systems with no reported companions. Our next paper in the series will feature AO images and astrometric measurements. We will also constrain the companion mass and separation for low-

mass companions below the detection limit. Additionally, we will identify the host stars based on transit duration and stellar density and recalculate planet radii by estimating the contrast between the two stars.

ACKNOWLEDGMENTS

J.Z. would like to thank Jerry Xuan, Pierre Kervella¹, and Michael Liu for helpful discussions. D.H. acknowledges support from the Alfred P. Sloan Foundation, the National Aeronautics and Space Administration (80NSSC21K0652), and the Australian Research Council (FT200100871). L.M.W. acknowledges support from the NASA-Keck Key Strategic Mission Support program (grant no. 80NSSC19K1475) and the NASA Exoplanet Research Program (grant no. 80NSSC23K0269). This work was supported by a NASA Keck PI Data Award, administered by the NASA Exoplanet Science Institute. Data presented herein were obtained at the W. M. Keck Observatory from telescope time allocated to the National Aeronautics and Space Administration through the agency’s scientific partnership with the California Institute of Technology and the University of California. The Observatory was made possible by the generous financial support of the W. M. Keck Foundation.

Some of the observations in this paper made use of the High-Resolution Imaging instruments ‘Alopeke and Zorro and were obtained under Gemini LLP Proposal Number: GN/S-2021A-LP-105. ‘Alopeke and Zorro were funded by the NASA Exoplanet Exploration Program and built at the NASA Ames Research Center by Steve B. Howell, Nic Scott, Elliott P. Horch, and Emmett Quigley. Alopeke was mounted on the Gemini

North telescope of the international Gemini Observatory, a program of NSF’s OIR Lab, which is managed by the Association of Universities for Research in Astronomy (AURA) under a cooperative agreement with the National Science Foundation. on behalf of the Gemini partnership: the National Science Foundation (United States), National Research Council (Canada), Agencia Nacional de Investigaci3n y Desarrollo (Chile), Ministerio de Ciencia, Tecnologí a e Innovaci3n (Argentina), Minist3rio da Ci3ncia, Tecnologia, Inovaes e Comunicaes (Brazil), and Korea Astronomy and Space Science Institute (Republic of Korea).

Funding for the TESS mission is provided by NASA’s Science Mission Directorate. This research has made use of the Exoplanet Follow-up Observation Program website, which is operated by the California Institute of Technology, under contract with the National Aeronautics and Space Administration under the Exoplanet Exploration Program.

This research has made use of the NASA Exoplanet Archive and ExoFOP, which are operated by the California Institute of Technology, under contract with the National Aeronautics and Space Administration under the Exoplanet Exploration Program.

The authors wish to recognize and acknowledge the very significant cultural role and reverence that the summit of Mauna Kea has always had within the indigenous Hawaiian community. We are most fortunate to have the opportunity to conduct observations from this mountain.

Facilities: *Kepler* , *TESS* , *Gaia* , *Hipparcos* , Keck:10m

Software: *orvara* (Brandt et al. 2021),

APPENDIX

A. NOTES ON FALSE POSITIVES IN THE TARGET SAMPLE

- HIP33681 (TOI-510): No obvious NEBs from SG1 but cannot yet clear very close neighbor.
- HIP15053 (TOI-394): TFOP SG1 identified different odd-even depth in TESS QLP light curve, which indicates that TOI394.01 is an EB. The RVs at two quadrature time collected using Keck/HIRES from the primary don’t show a RV difference consistent with a stellar mass object. So it is likely that the primary is orbited by a close EB companion and the transit is from the companion pair instead of the primary.
- HIP21952(TOI-271): TFOP SG1 finds no NEBs.
- HIP98516 (TOI-1124): TFOP SG1 detected event on target. But TFOP SG1 also detected strong chromaticity of the transit depth and odd-even depth in TESS light curve, which indicates TOI-1124.01 is a blend.
- HIP28122 (TOI-896): TFOP SG1 evaluated it as false alarm because of marginal signal. No transiting events are detected in sector 33, therefore TOI-896.01 retired as false alarm.

- HIP83168 (TOI-1418): TFOP SG1 identified multi-sector data seem more consistent with stellar variability.
- HIP58234 (TOI-680): SG1 clears the field of NEBs, and detects a 1ppt event arriving a little early. Additional transits show chromaticity, and HIRES RVs show no convincing variation phased to the ephemeris. This is likely a blend or a planet around the companion.
- HIP210000 (TOI-953): TFOP SG1 notes that WASP follow-up RVs show this to be an EB.
- HIP22084 (TOI-4314): TOI4314.01 has a long period of 73 days. TFOP SG1 note that the transits have low SNRs and possibly came from stellar variability.
- HIP79105 (TOI-2118): TFOP SG1 finds NEB 43" E.
- HIP55069 (TOI-1204): No obvious NEB in the SG1 sheet.
- HIP70833 (TOI-1946): TOI1946.01 retired as TFOP FP/NEB.
- HIP27844 (TOI-1665): TFOP SG1 finds NEB 32" E.
- HIP67650 (TOI-1837): TFOP SG1 notes that TRES+FIES RVs reveal 33 km/s variation consistent with stellar companion.
- HIP45621 (TOI-2666): TOI2666.01 is a single transit. Keck/HIRES spectra show that the star is a spectroscopic binary (SB). The companion is 18.5% the brightness of the secondary and separated by 35 km/s.
- HIP13754 (TOI-179): TFOP SG1 detects event on target
- HIP108162 (TOI-1099): TFOP SG1 detects event on target.
- HIP57386 (TOI-5521): There are no SG1 results available for this system. However, two TRES observations indicate a velocity offset of 29.5 km/s that is out of phase with the photometric ephemeris. This strongly suggests the presence of a stellar companion in the system, although it cannot be responsible for the shallow transits observed. This is consistent with the WDS catalog, which presents a companion at 0.7'' to TOI-5521.
- HIP93711 (TOI-2299): Possible on target. SG1 detected the transit, but it is unclear whether it originated from the target or a neighbor at 3.6 arcsec to the west. In addition, spoc-s14-s60 detects two TCEs at 214 and 246 days instead of a single TCE at 165 days. But they may not be reliable.
- HIP57990 (TOI-635): TFOP SG1 notes that TOI-634, TOI-635, TOI-638 all have similar ephemeris. Possible false alarm.
- HIP65205 (TOI-1831): It's a large star with a close companion at 0.66 arcsecs. The transit shows a slight odd-even transit depth difference, which could possibly come from an EB. SG1 clears the field of NEBs. But TRES observation does not find a large RV variation, so it retired as an APC/EB?/CRV in SG1. However, as there is a very close companion at 0.66 arcsec from the star, it is also possible that the transit event is occurring at the companion, which could explain why large RV variations were not seen in the primary star. We plan to investigate this system further in our project.
- HIP24718 (TOI-128): TFOP SG1 finds no NEBs beyond 2'' but they cannot rule out the close companion at $\sim 2''$. If the signal originates from either the primary star or companion, it could still be a planet.
- HIP82032 (TOI-909): TFOP SG1 detects an NEB on a nearby, $\Delta T=6.3$ star, TIC 1310226289. This is consistent with the SPOC centroids.
- HIP41849 (TOI-575): TFOP SG1 notes additional TESS data reveal this to be an EB, with primaries and secondaries both visible. Probably on a 0.6" companion seen in high-resolution imaging.
- HIP74685 (TOI-2017): TFOP SG1 detects event on target. But TOI2017.01 is an F+M EB with an orbital solution from TRES and the CfA Digital Speedometers.

- HIP118045 (TOI-222): TFOP SG1 identified as Spectroscopic Eclipsing Binary(SEB2).
- HIP40694 (TOI-522): TFOP SG1 clears the field of NEBs. HIP40694 is a rapid rotator, with a $v \sin i$ of 151 km/s.
- HIP54491 (TOI-1799): TFOP SG1 clears the field of NEBs.
- HIP78301 (TOI-906): TFOP SG1 detects event in aperture also containing 1", $\Delta T=2.9$ companion.
- HIP94780 (K06139): Kepler Eclipsing Binary Catalog v2 (Slawson et al. 2011) marks K06139.01 as an EB.
- HIP96501 (K01924): KOI 1924.01 is a false positive due to an eclipsing binary 77 arcseconds away.
- HIP93954 (K06364): Kepler Eclipsing Binary Catalog v2 (Slawson et al. 2011) marks K06364.01 as an EB.
- HIP80474 (EPIC204165788): Barros et al. (2016) marks it as eclipsing binary.
- HIP54766 (EPIC201488365): Armstrong et al. (2015) marks it as eclipsing binary.
- HIP41431 (EPIC212096658): Kruse et al. (2019) marks it as eclipsing binary.
- HIP78977 (EPIC204506777): Rizzuto et al. (2017) marks it as eclipsing binary.

B. LTT 1445 MCMC FITTING PLOTS

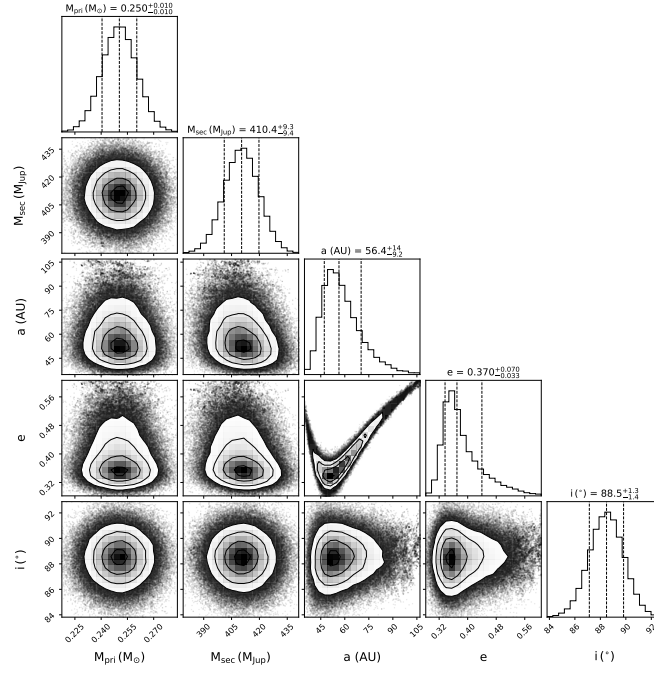


Figure B.1. Joint posterior distributions for selected orbital parameters of LTT 1445 BC. These are the host star’s mass (M_{pri}), the companion mass (M_{sec}), the semi-major axis a , the orbital eccentricity e , and the orbital inclination i . The values and histogram distributions of the posteriors of selected parameters are shown, along with 1σ uncertainties.

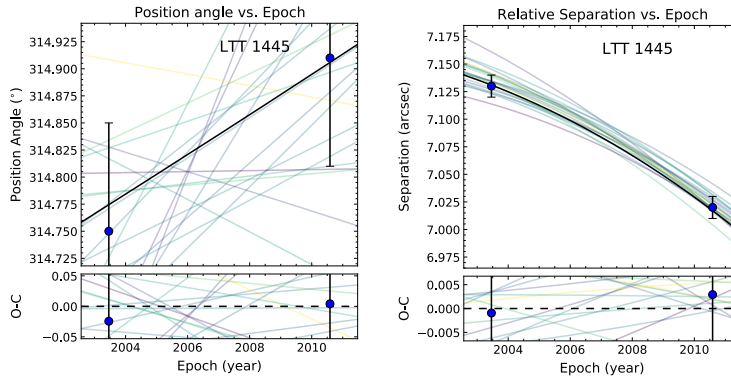


Figure B.2. Observed and fitted absolute astrometry for the LTT 1445 system. The two panels show the position angle and relative separation of LTT 1445 BC. The thicker black lines represent the best-fit orbit in the MCMC chain while the other 20 lines represent random draws from the chain.

C. TOIS WITH INSIGNIFICANT PROPER MOTION ANOMALIES ($\text{SNR}_G < 3$) WITHIN 300 PC**Table 5.** TOIs with low-SNR proper motion anomalies

Name	HIP Number	P_{pl} days	Exoplanet Archive Disposition	Δv_G $m s^{-1}$	SNR_G	distance pc
TOI 1011	36964	2.47	PC	3.81	0.47	52.38
TOI 1014	33170	1.41	PC	65.65	1.27	219.9
TOI 1025	46594	9.68	PC	19.66	0.34	130.12
TOI 1028	51271	1.02	FP	4.33	1.18	23.74
TOI 1029	27969	36.22	FP	22.25	2.09	68.69
TOI 1053	95348	5.74	FP	76.28	0.82	266.02
TOI 1054	99212	15.51	CP	14.43	1.02	89.05
TOI 1055	96160	17.47	CP	6.81	0.74	56.79
TOI 1097	61723	9.19	CP	18.23	1.45	79.56
TOI 1097	61723	13.9	CP	18.23	1.45	79.56
TOI 1098	62662	10.18	CP	15.4	0.89	105.14
TOI 1104	91434	341.28	PC	103.48	1.64	68.51
TOI 1127	95774	2.32	FP	35.04	0.8	174.91
TOI 1135	62908	8.03	PC	13.44	0.71	114.18
TOI 1148	52796	5.55	KP	9.68	0.59	96.88
TOI 1150	101252	1.48	KP	16.27	0.42	207.22
TOI 119	31609	5.54	PC	9.89	0.71	66.76
TOI 119	31609	10.69	PC	9.89	0.71	66.76
TOI 120	1419	11.54	CP	19.46	1.53	80.04
TOI 1203	54779	25.52	CP	2.93	0.28	64.96
TOI 1207	37931	2.63	PC	29.16	1.16	113.76
TOI 1233	60689	14.18	CP	12.12	1.37	64.57
TOI 1233	60689	19.59	CP	12.12	1.37	64.57
TOI 1233	60689	6.2	CP	12.12	1.37	64.57
TOI 1233	60689	3.8	CP	12.12	1.37	64.57
TOI 1247	74326	15.92	PC	21.43	1.76	73.39
TOI 1250	88071	1.44	FA	39.3	1.44	66.44
TOI 1255	97166	10.29	CP	11.41	0.97	66.04
TOI 129	65	0.98	CP	42.74	2.43	61.87
TOI 130	3911	14.34	CP	12.34	1.13	57.41
TOI 134	115211	1.4	CP	16.69	1.68	25.18
TOI 1354	102712	1.43	FP	323.06	1.94	248.45
TOI 1355	109028	2.17	PC	34.12	0.82	250.08
TOI 139	110692	11.07	PC	31.29	2.52	42.42
TOI 1407	110758	9.98	KP	14.42	0.77	80.5
TOI 1411	76042	1.45	CP	17.1	2.32	32.46
TOI 1415	71409	14.42	PC	35.65	2.03	111.98
TOI 1416	70705	1.07	PC	9.71	0.85	55.04
TOI 1430	98668	7.43	PC	3.88	0.57	41.24
TOI 1431	104051	2.65	CP	47.14	1.87	149.59
TOI 1434	57350	29.9	PC	9.64	1.52	37.81
TOI 1440	92848	15.52	PC	161.27	1.94	236.48
TOI 1440	92848	4.63	PC	161.27	1.94	236.48
TOI 1462	85268	2.18	CP	6.89	1.46	27.01

Name	HIP Number	P_{pl} days	Exoplanet Archive Disposition ^a	Δv_G $m s^{-1}$	SNR _G	distance pc
TOI 1471	9618	20.77	PC	23.86	1.66	67.29
TOI 1471	9618	683.33	PC	23.86	1.66	67.29
TOI 1475	117382	8.5	PC	32.14	0.75	289.64
TOI 1487	83359	23.29	FA	14.66	0.62	109.73
TOI 1488	85444	0.47	FA	63.85	2.34	159.7
TOI 1514	115710	1.37	FP	123.97	2.77	239.68
TOI 1573	13192	21.22	KP	30.16	2.56	77.43
TOI 1599	11397	1.22	KP	43.04	1.34	121.6
TOI 1608	15767	2.47	APC	3.96	0.15	101.29
TOI 1611	107038	16.2	CP	5.13	1.1	28.28
TOI 1652	61278	0.67	PC	23.65	1.27	129.3
TOI 1682	24323	2.73	KP	14.76	0.72	135.52
TOI 1683	20528	3.06	PC	43.52	2.16	50.94
TOI 1689	84062	9.12	PC	48.89	0.4	28.02
TOI 1718	36272	5.59	PC	8.34	0.82	52.06
TOI 1726	38228	7.11	CP	9.75	2.39	22.38
TOI 1726	38228	20.54	CP	9.75	2.39	22.38
TOI 173	10389	29.75	PC	27.7	1.05	150.07
TOI 174	17264	17.67	CP	1.14	0.14	39.09
TOI 174	17264	29.8	CP	1.14	0.14	39.09
TOI 174	17264	12.16	CP	1.14	0.14	39.09
TOI 174	17264	3.98	CP	1.14	0.14	39.09
TOI 174	17264	7.91	CP	1.14	0.14	39.09
TOI 177	6365	2.85	CP	4.15	0.44	22.45
TOI 1773	43587	0.74	KP	4.35	1.18	12.59
TOI 1774	48443	16.71	CP	10.68	1.02	53.84
TOI 1776	53688	2.8	PC	8.38	0.87	44.75
TOI 1777	49576	14.65	PC	15.73	0.77	80.14
TOI 1778	44746	6.52	PC	41.16	1.64	99.31
TOI 1793	53719	55.09	CP	10.92	1.74	36.97
TOI 180	4460	0.84	APC	159.24	2.21	259.7
TOI 1801	57099	10.64	PC	16.67	1.12	30.89
TOI 1807	65469	0.55	CP	14.14	1.66	42.59
TOI 1821	54906	9.49	KP	1.72	0.42	21.56
TOI 1827	62452	1.47	CP	4.12	1.06	8.08
TOI 1830	73765	9.78	FP	19.35	2.74	50.31
TOI 185	7562	0.94	KP	55.25	2.63	122.79
TOI 186	16069	35.61	CP	2.26	0.51	16.33
TOI 186	16069	7.79	CP	2.26	0.51	16.33
TOI 1860	73869	1.07	CP	5.4	0.74	45.74
TOI 1898	47288	45.52	PC	43.35	2.52	80.13
TOI 193	117883	0.79	CP	12.65	0.8	81.05
TOI 196	4548	1.16	PC	100.38	2.26	290.64
TOI 1969	72490	2.69	FP	45.06	2.28	106.82
TOI 197	116158	14.28	CP	6.35	0.27	95.43
TOI 198	738	10.22	PC	11.5	1.5	23.78
TOI 200	116748	8.14	CP	24.44	2.78	44.18
TOI 2009	5286	nan	PC	13.94	2.42	20.54

Name	HIP Number	P_{pl} days	Exoplanet Archive Disposition ^a	Δv_G $m s^{-1}$	SNR _G	distance pc
TOI 2018	74981	7.44	PC	4.7	0.73	28.04
TOI 2020	80076	5.63	KP	12.17	0.63	128.52
TOI 2024	80838	2.88	KP	9.31	0.77	76.22
TOI 2056	848	10.22	PC	15.34	1.1	92.74
TOI 2069	80243	5.92	PC	10.33	1.74	38.61
TOI 2082	78892	30.2	PC	23.37	2.35	63.74
TOI 2091	86067	177.22	PC	10.72	0.9	70.39
TOI 2105	58868	15.92	PC	33.36	1.84	72.89
TOI 2111	84840	1.27	FP	35.33	2.74	83.16
TOI 2112	113195	14.01	PC	9.16	0.69	86.17
TOI 2112	113195	155.82	PC	9.16	0.69	86.17
TOI 2115	6105	3.69	FP	13.0	0.27	215.64
TOI 2128	83827	16.34	PC	4.49	0.93	36.67
TOI 214	31692	18.55	PC	13.43	1.11	38.94
TOI 214	31692	9.7	PC	13.43	1.11	38.94
TOI 2145	86040	10.26	CP	49.45	1.36	226.24
TOI 2194	98130	15.34	PC	1.97	0.42	19.55
TOI 2211	101503	3.09	PC	3.86	0.19	70.45
TOI 2221	102409	nan	CP	2.48	1.05	9.71
TOI 2259	79876	16.59	PC	39.79	2.09	121.94
TOI 2270	79823	nan	PC	4.37	0.29	94.23
TOI 2301	74576	6.05	PC	23.7	1.28	119.01
TOI 2431	11707	0.22	PC	15.13	1.1	36.01
TOI 2443	12493	15.67	PC	5.98	0.9	23.91
TOI 245	113831	8.77	PC	80.43	2.27	125.06
TOI 2474	24830	4.28	PC	40.22	1.21	132.43
TOI 248	10779	5.99	PC	7.95	0.68	76.09
TOI 253	4468	3.51	PC	3.02	0.32	30.91
TOI 2540	25775	12.72	PC	4.15	0.51	19.16
TOI 2540	25775	22.08	APC	4.15	0.51	19.16
TOI 257	14710	18.39	CP	21.14	1.85	76.86
TOI 260	1532	13.48	PC	4.27	0.88	20.21
TOI 261	4739	3.36	PC	28.81	0.9	113.64
TOI 261	4739	13.04	CP	28.81	0.9	113.64
TOI 262	10117	11.15	CP	3.72	0.43	44.14
TOI 266	8152	10.75	PC	4.92	0.23	101.69
TOI 266	8152	6.19	PC	4.92	0.23	101.69
TOI 282	20295	56.01	CP	16.46	0.74	140.24
TOI 282	20295	31.32	FA	16.46	0.74	140.24
TOI 282	20295	84.26	CP	16.46	0.74	140.24
TOI 282	20295	22.89	CP	16.46	0.74	140.24
TOI 381	7060	4.9	FP	14.48	1.42	75.3
TOI 387	16212	4.16	FP	37.28	0.56	218.8
TOI 389	36612	13.46	FP	20.69	1.16	105.0
TOI 396	13363	5.97	CP	6.67	1.01	31.7
TOI 396	13363	3.59	CP	6.67	1.01	31.7
TOI 396	13363	11.23	CP	6.67	1.01	31.7
TOI 409	33392	6.8	FP	16.24	1.46	53.27

Name	HIP Number	P_{pl} days	Exoplanet Archive Disposition ^a	Δv_G $m s^{-1}$	SNR _G	distance pc
TOI 411	17047	9.57	CP	6.89	0.6	62.9
TOI 411	17047	4.04	CP	6.89	0.6	62.9
TOI 4186	105697	12.76	PC	42.92	2.22	67.61
TOI 4187	14982	30.88	PC	45.53	1.99	154.81
TOI 4189	25359	46.96	PC	6.95	0.63	69.31
TOI 419	33390	0.4	FP	14.45	0.41	42.59
TOI 4191	49531	742.86	PC	19.91	1.06	83.73
TOI 430	18761	0.59	FP	23.17	1.61	66.09
TOI 4302	4599	38.76	PC	82.56	2.61	132.22
TOI 4303	22414	8.61	PC	42.0	0.96	253.4
TOI 4304	41378	15.57	KP	30.64	1.22	105.98
TOI 4304	41378	31.72	KP	30.64	1.22	105.98
TOI 4305	102133	183.0	PC	14.12	0.51	161.04
TOI 4305	102133	374.36	PC	14.12	0.51	161.04
TOI 4307	25351	32.7	PC	1.48	0.31	36.12
TOI 4307	25351	4.65	PC	1.48	0.31	36.12
TOI 4309	51743	87.22	PC	37.57	2.23	76.06
TOI 431	26013	12.46	CP	4.22	0.85	32.62
TOI 431	26013	0.49	CP	4.22	0.85	32.62
TOI 4320	16038	703.62	PC	11.45	0.85	79.43
TOI 4320	16038	46.41	FA	11.45	0.85	79.43
TOI 4321	107911	nan	PC	15.13	0.84	109.32
TOI 4324	47619	6.25	PC	10.41	1.43	17.06
TOI 4326	115828	nan	PC	15.94	1.3	57.77
TOI 4328	21223	703.79	PC	3.9	0.83	25.02
TOI 4330	71815	3.35	PC	138.19	1.76	287.19
TOI 4337	53534	2.29	PC	8.32	0.54	64.83
TOI 4350	10229	4.88	PC	4.93	0.26	103.38
TOI 4355	31179	674.23	PC	19.65	1.62	76.36
TOI 4358	113293	390.46	PC	27.66	2.23	66.28
TOI 4362	34209	7.55	PC	19.13	0.92	134.6
TOI 4369	32099	13.58	PC	197.03	0.25	283.99
TOI 4382	86844	10.69	PC	145.03	2.79	166.34
TOI 440	25670	1.08	FP	12.13	1.33	49.37
TOI 444	19950	17.96	PC	5.34	0.41	57.45
TOI 4470	98505	2.22	KP	6.37	2.58	19.78
TOI 4481	102401	0.93	PC	4.92	1.5	12.06
TOI 4498	96902	5.31	FP	42.77	2.8	79.83
TOI 4517	115752	1.21	KP	25.89	2.84	29.65
TOI 4524	15249	0.93	CP	14.19	1.06	63.86
TOI 4527	6069	0.4	PC	12.56	0.48	18.1
TOI 4537	112100	6.66	PC	35.06	2.66	70.61
TOI 454	15407	18.08	APC	19.11	1.25	79.03
TOI 4580	79180	0.92	PC	2.34	0.24	67.65
TOI 4588	92247	13.12	PC	14.07	0.35	226.82
TOI 4597	22838	4.67	PC	66.83	2.82	124.2
TOI 4599	31635	2.77	CP	1.28	0.49	10.0
TOI 4599	31635	5.71	CP	1.28	0.49	10.0

Name	HIP Number	P_{pl} days	Exoplanet Archive Disposition ^a	Δv_G $m s^{-1}$	SNR _G	distance pc
TOI 4602	18841	3.98	PC	12.48	1.18	62.81
TOI 461	11865	10.92	PC	14.14	1.22	45.74
TOI 4612	29301	4.11	KP	10.87	0.46	134.54
TOI 4626	66854	17.48	PC	12.13	1.21	51.15
TOI 4631	45012	33.64	PC	15.48	1.52	62.26
TOI 4641	13224	22.1	PC	31.72	1.87	87.65
TOI 469	29442	13.63	CP	24.04	2.03	68.0
TOI 480	27849	6.87	PC	22.21	2.84	54.28
TOI 486	31300	1.74	PC	4.28	0.76	15.22
TOI 500	34269	0.55	CP	7.15	0.71	47.41
TOI 5076	15683	23.44	PC	33.03	1.05	82.75
TOI 5082	34271	4.24	PC	10.69	0.98	43.03
TOI 509	38374	9.06	CP	13.6	1.23	48.85
TOI 509	38374	21.4	CP	13.6	1.23	48.85
TOI 5099	13913	14.45	PC	70.32	2.65	91.99
TOI 5108	54186	6.75	PC	67.85	1.48	130.97
TOI 5125	27695	5.91	PC	24.13	0.57	165.4
TOI 5128	46885	7.6	PC	70.07	1.08	192.93
TOI 5141	50496	11.81	KP	48.13	1.68	131.36
TOI 5156	17668	22.85	PC	178.84	1.75	159.46
TOI 5384	51260	2.99	KP	20.02	0.26	218.06
TOI 5387	69858	2.8	PC	22.15	1.03	141.19
TOI 5392	69240	17.53	PC	21.85	2.22	48.51
TOI 5394	50469	15.19	PC	43.9	2.88	64.18
TOI 5401	61637	6.83	PC	137.4	1.4	216.55
TOI 554	18893	7.05	PC	2.83	0.31	45.18
TOI 554	18893	3.04	PC	2.83	0.31	45.18
TOI 560	42401	6.4	CP	10.09	1.36	31.59
TOI 560	42401	18.88	CP	10.09	1.36	31.59
TOI 562	47103	3.93	CP	4.34	1.86	9.44
TOI 5724	80264	697.4	PC	1.9	0.26	50.4
TOI 5739	66730	8.43	PC	19.63	1.87	61.84
TOI 5789	99452	12.93	PC	2.52	0.9	20.44
TOI 5807	101511	14.24	PC	10.79	1.12	73.06
TOI 5809	103502	9.21	PC	229.51	1.73	38.67
TOI 5817	106097	15.61	PC	16.37	1.09	80.34
TOI 5821	104513	2.15	KP	98.31	2.73	182.19
TOI 585	43991	5.55	APC	24.1	0.94	157.55
TOI 587	42654	8.04	PC	37.57	0.96	210.31
TOI 588	33609	39.47	PC	63.0	1.98	151.88
TOI 5951	113300	3.17	PC	65.87	2.72	160.83
TOI 5955	116907	0.59	PC	58.48	1.95	43.07
TOI 5961	114941	1.62	PC	9.09	1.18	26.29
TOI 5972	108859	3.52	KP	7.35	0.7	48.15
TOI 5997	85850	5.66	PC	21.2	2.07	46.62
TOI 6026	74	1.28	PC	8.73	1.2	42.0
TOI 6054	17540	7.49	PC	24.03	1.64	78.73
TOI 6054	17540	12.58	PC	24.03	1.64	78.73

Name	HIP Number	P_{pl} days	Exoplanet Archive Disposition ^a	Δv_G $m s^{-1}$	SNR _G	distance pc
TOI 6075	91906	832.92	PC	7.89	0.84	39.88
TOI 6098	38729	2.73	PC	27.15	2.18	81.72
TOI 651	29118	1.07	PC	30.07	2.03	85.86
TOI 652	48739	3.98	CP	9.51	1.02	45.6
TOI 653	47371	0.69	FP	94.5	1.99	213.86
TOI 664	52733	4.74	KP	10.75	0.48	99.95
TOI 704	28754	3.81	CP	2.78	0.21	29.8
TOI 731	47780	0.32	CP	19.11	1.64	9.42
TOI 740	49678	2.13	PC	21.34	0.87	114.55
TOI 741	45908	7.58	PC	0.46	0.23	10.45
TOI 755	61820	2.54	CP	38.19	1.64	105.82
TOI 801	32674	0.78	PC	21.42	1.73	71.4
TOI 802	31134	3.69	PC	1.31	0.26	28.06
TOI 836	73427	8.6	CP	9.38	1.19	27.51
TOI 836	73427	3.82	PC	9.38	1.19	27.51
TOI 869	16521	26.48	FA	26.0	1.36	110.53
TOI 911	85583	8.58	APC	60.76	2.94	85.17
TOI 957	24689	0.83	FP	39.77	0.64	275.31

^a The flags come from NASA Exoplanet Archive. CP: Confirmed Planet, PC: Planet Candidate, APC: Ambiguous Planet Candidate, FP: False Positive, FA: False Alarm.

REFERENCES

- 1997, ESA Special Publication, Vol. 1200, The HIPPARCOS and TYCHO catalogues. Astrometric and photometric star catalogues derived from the ESA HIPPARCOS Space Astrometry Mission
- Adams, F. C., Ruden, S. P., & Shu, F. H. 1989, *ApJ*, 347, 959, doi: [10.1086/168187](https://doi.org/10.1086/168187)
- Akeson, R. L., Jensen, E. L. N., Carpenter, J., et al. 2019, *ApJ*, 872, 158, doi: [10.3847/1538-4357/aaff6a](https://doi.org/10.3847/1538-4357/aaff6a)
- Armstrong, D. J., Kirk, J., Lam, K. W. F., et al. 2015, *A&A*, 579, A19, doi: [10.1051/0004-6361/201525889](https://doi.org/10.1051/0004-6361/201525889)
- Artymowicz, P., & Lubow, S. H. 1994, *ApJ*, 421, 651, doi: [10.1086/173679](https://doi.org/10.1086/173679)
- Badenas-Agusti, M., Günther, M. N., Daylan, T., et al. 2020, *AJ*, 160, 113, doi: [10.3847/1538-3881/aba0b5](https://doi.org/10.3847/1538-3881/aba0b5)
- Barros, S. C. C., Demangeon, O., & Deleuil, M. 2016, *A&A*, 594, A100, doi: [10.1051/0004-6361/201628902](https://doi.org/10.1051/0004-6361/201628902)
- Batalha, N. M., Rowe, J. F., Bryson, S. T., et al. 2013, *ApJS*, 204, 24, doi: [10.1088/0067-0049/204/2/24](https://doi.org/10.1088/0067-0049/204/2/24)
- Borucki, W. J., Koch, D., Basri, G., et al. 2010, *Science*, 327, 977, doi: [10.1126/science.1185402](https://doi.org/10.1126/science.1185402)
- Brandt, T. D. 2021, *ApJS*, 254, 42, doi: [10.3847/1538-4365/abf93c](https://doi.org/10.3847/1538-4365/abf93c)
- Brandt, T. D., Dupuy, T. J., & Bowler, B. P. 2019, *AJ*, 158, 140, doi: [10.3847/1538-3881/ab04a8](https://doi.org/10.3847/1538-3881/ab04a8)
- Brandt, T. D., Dupuy, T. J., Li, Y., et al. 2021, *orvara: Orbits from Radial Velocity, Absolute, and/or Relative Astrometry*. <http://ascl.net/2105.012>
- Burke, C. J., Bryson, S. T., Mullally, F., et al. 2014, *ApJS*, 210, 19, doi: [10.1088/0067-0049/210/2/19](https://doi.org/10.1088/0067-0049/210/2/19)
- Cadman, J., Hall, C., Fontanive, C., & Rice, K. 2022, *MNRAS*, 511, 457, doi: [10.1093/mnras/stac033](https://doi.org/10.1093/mnras/stac033)
- Campante, T. L., Barclay, T., Swift, J. J., et al. 2015, *ApJ*, 799, 170, doi: [10.1088/0004-637X/799/2/170](https://doi.org/10.1088/0004-637X/799/2/170)
- Correia, A. C. M., Udry, S., Mayor, M., et al. 2008, *A&A*, 479, 271, doi: [10.1051/0004-6361:20078908](https://doi.org/10.1051/0004-6361:20078908)
- Coughlin, J. L., Mullally, F., Thompson, S. E., et al. 2016, *ApJS*, 224, 12, doi: [10.3847/0067-0049/224/1/12](https://doi.org/10.3847/0067-0049/224/1/12)
- Cox, E. G., Harris, R. J., Looney, L. W., et al. 2017, *ApJ*, 851, 83, doi: [10.3847/1538-4357/aa97e2](https://doi.org/10.3847/1538-4357/aa97e2)
- Cumming, A., Butler, R. P., Marcy, G. W., et al. 2008, *PASP*, 120, 531, doi: [10.1086/588487](https://doi.org/10.1086/588487)
- Damasso, M., Sozzetti, A., Lovis, C., et al. 2020, *A&A*, 642, A31, doi: [10.1051/0004-6361/202038416](https://doi.org/10.1051/0004-6361/202038416)
- De Rosa, R. J., Dawson, R., & Nielsen, E. L. 2020, *A&A*, 640, A73, doi: [10.1051/0004-6361/202038496](https://doi.org/10.1051/0004-6361/202038496)
- Dieterich, S. B., Henry, T. J., Golimowski, D. A., Krist, J. E., & Tanner, A. M. 2012, *AJ*, 144, 64, doi: [10.1088/0004-6256/144/2/64](https://doi.org/10.1088/0004-6256/144/2/64)
- Dumusque, X., Turner, O., Dorn, C., et al. 2019, *A&A*, 627, A43, doi: [10.1051/0004-6361/201935457](https://doi.org/10.1051/0004-6361/201935457)
- Dupuy, T. J., Kratter, K. M., Kraus, A. L., et al. 2016, *ApJ*, 817, 80, doi: [10.3847/0004-637X/817/1/80](https://doi.org/10.3847/0004-637X/817/1/80)
- Dupuy, T. J., Kraus, A. L., Kratter, K. M., et al. 2022, *MNRAS*, 512, 648, doi: [10.1093/mnras/stac306](https://doi.org/10.1093/mnras/stac306)
- Fontanive, C., & Bardalez Gagliuffi, D. 2021, *Frontiers in Astronomy and Space Sciences*, 8, 16, doi: [10.3389/fspas.2021.625250](https://doi.org/10.3389/fspas.2021.625250)
- Fulton, B. J., Rosenthal, L. J., Hirsch, L. A., et al. 2021, *ApJS*, 255, 14, doi: [10.3847/1538-4365/abfcc1](https://doi.org/10.3847/1538-4365/abfcc1)
- Furlan, E., Ciardi, D. R., Everett, M. E., et al. 2017, *AJ*, 153, 71, doi: [10.3847/1538-3881/153/2/71](https://doi.org/10.3847/1538-3881/153/2/71)
- Gaia Collaboration, Klioner, S. A., Lindegren, L., et al. 2022, *arXiv e-prints*, arXiv:2204.12574. <https://arxiv.org/abs/2204.12574>
- Gandolfi, D., Barragán, O., Livingston, J. H., et al. 2018, *A&A*, 619, L10, doi: [10.1051/0004-6361/201834289](https://doi.org/10.1051/0004-6361/201834289)
- Gandolfi, D., Fossati, L., Livingston, J. H., et al. 2019, *ApJL*, 876, L24, doi: [10.3847/2041-8213/ab17d9](https://doi.org/10.3847/2041-8213/ab17d9)
- Guerrero, N. M., Seager, S., Huang, C. X., et al. 2021, *ApJS*, 254, 39, doi: [10.3847/1538-4365/abefel](https://doi.org/10.3847/1538-4365/abefel)
- Hatzes, A. P., Cochran, W. D., Endl, M., et al. 2003, *ApJ*, 599, 1383, doi: [10.1086/379281](https://doi.org/10.1086/379281)
- Hatzes, A. P., Gandolfi, D., Korth, J., et al. 2022, *AJ*, 163, 223, doi: [10.3847/1538-3881/ac5dcb](https://doi.org/10.3847/1538-3881/ac5dcb)
- Hirsch, L. A., Rosenthal, L., Fulton, B. J., et al. 2021, *AJ*, 161, 134, doi: [10.3847/1538-3881/abd639](https://doi.org/10.3847/1538-3881/abd639)
- Hobson, M. J., Brahm, R., Jordán, A., et al. 2021, *AJ*, 161, 235, doi: [10.3847/1538-3881/abeaa1](https://doi.org/10.3847/1538-3881/abeaa1)
- Howard, A. W., Marcy, G. W., Bryson, S. T., et al. 2012, *ApJS*, 201, 15, doi: [10.1088/0067-0049/201/2/15](https://doi.org/10.1088/0067-0049/201/2/15)
- Howell, S. B., Matson, R. A., Ciardi, D. R., et al. 2021, *AJ*, 161, 164, doi: [10.3847/1538-3881/abdec6](https://doi.org/10.3847/1538-3881/abdec6)
- Howell, S. B., Sobeck, C., Haas, M., et al. 2014, *PASP*, 126, 398, doi: [10.1086/676406](https://doi.org/10.1086/676406)
- Huber, D., Carter, J. A., Barbieri, M., et al. 2013, *Science*, 342, 331, doi: [10.1126/science.1242066](https://doi.org/10.1126/science.1242066)
- Huber, D., Bryson, S. T., Haas, M. R., et al. 2016, *ApJS*, 224, 2, doi: [10.3847/0067-0049/224/1/2](https://doi.org/10.3847/0067-0049/224/1/2)
- Jang-Condell, H., Chen, C., Nesvold, E., et al. 2015, in *American Astronomical Society Meeting Abstracts*, Vol. 225, American Astronomical Society Meeting Abstracts #225, 330.04
- Jones, H. R. A., Paul Butler, R., Tinney, C. G., et al. 2002, *MNRAS*, 333, 871, doi: [10.1046/j.1365-8711.2002.05459.x](https://doi.org/10.1046/j.1365-8711.2002.05459.x)
- Kane, S. R., Barclay, T., Hartmann, M., et al. 2015, *ApJ*, 815, 32, doi: [10.1088/0004-637X/815/1/32](https://doi.org/10.1088/0004-637X/815/1/32)

- Kervella, P., Arenou, F., Mignard, F., & Thévenin, F. 2019, *A&A*, 623, A72, doi: [10.1051/0004-6361/201834371](https://doi.org/10.1051/0004-6361/201834371)
- Kostov, V. B., Mullally, S. E., Quintana, E. V., et al. 2019, *AJ*, 157, 124, doi: [10.3847/1538-3881/ab0110](https://doi.org/10.3847/1538-3881/ab0110)
- Kozai, Y. 1962, *AJ*, 67, 591, doi: [10.1086/108790](https://doi.org/10.1086/108790)
- Kraus, A. L., Ireland, M. J., Huber, D., Mann, A. W., & Dupuy, T. J. 2016, *AJ*, 152, 8, doi: [10.3847/0004-6256/152/1/8](https://doi.org/10.3847/0004-6256/152/1/8)
- Kruse, E., Agol, E., Luger, R., & Foreman-Mackey, D. 2019, *ApJS*, 244, 11, doi: [10.3847/1538-4365/ab346b](https://doi.org/10.3847/1538-4365/ab346b)
- Lavie, B., Bouchy, F., Lovis, C., et al. 2022, arXiv e-prints, arXiv:2210.09713, doi: [10.48550/arXiv.2210.09713](https://doi.org/10.48550/arXiv.2210.09713)
- Lester, K. V., Matson, R. A., Howell, S. B., et al. 2021, *AJ*, 162, 75, doi: [10.3847/1538-3881/ac0d06](https://doi.org/10.3847/1538-3881/ac0d06)
- Lidov, M. L. 1962, *Planet. Space Sci.*, 9, 719, doi: [10.1016/0032-0633\(62\)90129-0](https://doi.org/10.1016/0032-0633(62)90129-0)
- Lindgren, L., Hernández, J., Bombrun, A., et al. 2018, *A&A*, 616, A2, doi: [10.1051/0004-6361/201832727](https://doi.org/10.1051/0004-6361/201832727)
- Lubin, J., Van Zandt, J., Holcomb, R., et al. 2022, *AJ*, 163, 101, doi: [10.3847/1538-3881/ac3d38](https://doi.org/10.3847/1538-3881/ac3d38)
- Luyten, W. J. 1957, A catalogue of 9867 stars in the Southern Hemisphere with proper motions exceeding 0."2 annually.
- . 1980, *NLTT Catalogue. Volume_III. 0__to -30_*.
- Manara, C. F., Tazzari, M., Long, F., et al. 2019, *A&A*, 628, A95, doi: [10.1051/0004-6361/201935964](https://doi.org/10.1051/0004-6361/201935964)
- Mason, B. D., Wycoff, G. L., Hartkopf, W. I., Douglass, G. G., & Worley, C. E. 2001, *AJ*, 122, 3466, doi: [10.1086/323920](https://doi.org/10.1086/323920)
- Mills, S. M., & Fabrycky, D. C. 2017, *ApJL*, 838, L11, doi: [10.3847/2041-8213/aa6543](https://doi.org/10.3847/2041-8213/aa6543)
- Moe, M., & Kratter, K. M. 2018, *ApJ*, 854, 44, doi: [10.3847/1538-4357/aaa6d2](https://doi.org/10.3847/1538-4357/aaa6d2)
- . 2021, *MNRAS*, 507, 3593, doi: [10.1093/mnras/stab2328](https://doi.org/10.1093/mnras/stab2328)
- Mullally, F., Coughlin, J. L., Thompson, S. E., et al. 2015, *ApJS*, 217, 31, doi: [10.1088/0067-0049/217/2/31](https://doi.org/10.1088/0067-0049/217/2/31)
- Offner, S. S. R., Moe, M., Kratter, K. M., et al. 2022, arXiv e-prints, arXiv:2203.10066, doi: [10.48550/arXiv.2203.10066](https://doi.org/10.48550/arXiv.2203.10066)
- Orell-Miquel, J., Nowak, G., Murgas, F., et al. 2023, *A&A*, 669, A40, doi: [10.1051/0004-6361/202244120](https://doi.org/10.1051/0004-6361/202244120)
- Paczynski, B. 1977, *ApJ*, 216, 822, doi: [10.1086/155526](https://doi.org/10.1086/155526)
- Perryman, M. A. C., Lindgren, L., Kovalevsky, J., et al. 1997, *A&A*, 323, L49
- Pichardo, B., Sparke, L. S., & Aguilar, L. A. 2005, *MNRAS*, 359, 521, doi: [10.1111/j.1365-2966.2005.08905.x](https://doi.org/10.1111/j.1365-2966.2005.08905.x)
- Pope, B. J. S., Parviainen, H., & Aigrain, S. 2016, *MNRAS*, 461, 3399, doi: [10.1093/mnras/stw1373](https://doi.org/10.1093/mnras/stw1373)
- Quintana, E. V., Adams, F. C., Lissauer, J. J., & Chambers, J. E. 2007, *ApJ*, 660, 807, doi: [10.1086/512542](https://doi.org/10.1086/512542)
- Raghavan, D., McAlister, H. A., Henry, T. J., et al. 2010, *ApJS*, 190, 1, doi: [10.1088/0067-0049/190/1/1](https://doi.org/10.1088/0067-0049/190/1/1)
- Ricker, G. R., Winn, J. N., Vanderspek, R., et al. 2014, in *Society of Photo-Optical Instrumentation Engineers (SPIE) Conference Series*, Vol. 9143, Space Telescopes and Instrumentation 2014: Optical, Infrared, and Millimeter Wave, ed. J. Oschmann, Jacobus M., M. Clampin, G. G. Fazio, & H. A. MacEwen, 914320, doi: [10.1117/12.2063489](https://doi.org/10.1117/12.2063489)
- Rizzuto, A. C., Mann, A. W., Vanderburg, A., Kraus, A. L., & Covey, K. R. 2017, *AJ*, 154, 224, doi: [10.3847/1538-3881/aa9070](https://doi.org/10.3847/1538-3881/aa9070)
- Rodríguez, D. R., Duchêne, G., Tom, H., et al. 2015, *MNRAS*, 449, 3160, doi: [10.1093/mnras/stv483](https://doi.org/10.1093/mnras/stv483)
- Rossiter, R. A. 1955, *Publications of Michigan Observatory*, 11, 1
- Rowe, J. F., Coughlin, J. L., Antoci, V., et al. 2015, *ApJS*, 217, 16, doi: [10.1088/0067-0049/217/1/16](https://doi.org/10.1088/0067-0049/217/1/16)
- Rudak, B., & Paczynski, B. 1981, *AcA*, 31, 13
- Simpson, A., & Cloutier, R. 2022, in *American Astronomical Society Meeting Abstracts*, Vol. 54, American Astronomical Society Meeting Abstracts, 403.10
- Slawson, R. W., Prša, A., Welsh, W. F., et al. 2011, *AJ*, 142, 160, doi: [10.1088/0004-6256/142/5/160](https://doi.org/10.1088/0004-6256/142/5/160)
- Sullivan, K., Kraus, A. L., Huber, D., et al. 2023, arXiv e-prints, arXiv:2302.08532, doi: [10.48550/arXiv.2302.08532](https://doi.org/10.48550/arXiv.2302.08532)
- Teske, J. K., Ciardi, D. R., Howell, S. B., Hirsch, L. A., & Johnson, R. A. 2018, *AJ*, 156, 292, doi: [10.3847/1538-3881/aaed2d](https://doi.org/10.3847/1538-3881/aaed2d)
- Thompson, S. E., Coughlin, J. L., Hoffman, K., et al. 2018, *ApJS*, 235, 38, doi: [10.3847/1538-4365/aab4f9](https://doi.org/10.3847/1538-4365/aab4f9)
- Trifonov, T., Tal-Or, L., Zechmeister, M., et al. 2020, *A&A*, 636, A74, doi: [10.1051/0004-6361/201936686](https://doi.org/10.1051/0004-6361/201936686)
- Wang, J., Fischer, D. A., Xie, J.-W., & Ciardi, D. R. 2015, *ApJ*, 813, 130, doi: [10.1088/0004-637X/813/2/130](https://doi.org/10.1088/0004-637X/813/2/130)
- Winters, J., Cloutier, R., Medina, A., et al. 2022, in *Bulletin of the American Astronomical Society*, Vol. 54, 102.417
- Winters, J. G., Medina, A. A., Irwin, J. M., et al. 2019, *AJ*, 158, 152, doi: [10.3847/1538-3881/ab364d](https://doi.org/10.3847/1538-3881/ab364d)
- Xuan, J. W., & Wyatt, M. C. 2020, *MNRAS*, 497, 2096, doi: [10.1093/mnras/staa2033](https://doi.org/10.1093/mnras/staa2033)
- Zagaria, F., Rosotti, G. P., Alexander, R. D., & Clarke, C. J. 2023, *European Physical Journal Plus*, 138, 25, doi: [10.1140/epjp/s13360-022-03616-4](https://doi.org/10.1140/epjp/s13360-022-03616-4)
- Zanazzi, J. J., & Lai, D. 2018, *MNRAS*, 477, 5207, doi: [10.1093/mnras/sty951](https://doi.org/10.1093/mnras/sty951)
- Zhang, J., Weiss, L. M., Huber, D., et al. 2021, *AJ*, 162, 89, doi: [10.3847/1538-3881/ac0634](https://doi.org/10.3847/1538-3881/ac0634)

- Zhang, Z., Bowler, B. P., Dupuy, T. J., et al. 2022, arXiv e-prints, arXiv:2210.07252.
<https://arxiv.org/abs/2210.07252>
- Zhou, G., Wirth, C. P., Huang, C. X., et al. 2022, AJ, 163, 289, doi: [10.3847/1538-3881/ac69e3](https://doi.org/10.3847/1538-3881/ac69e3)
- Ziegler, C., Tokovinin, A., Briceño, C., et al. 2020, AJ, 159, 19, doi: [10.3847/1538-3881/ab55e9](https://doi.org/10.3847/1538-3881/ab55e9)
- Ziegler, C., Tokovinin, A., Latiolais, M., et al. 2021, AJ, 162, 192, doi: [10.3847/1538-3881/ac17f6](https://doi.org/10.3847/1538-3881/ac17f6)
- Zink, J. K., Hardegree-Ullman, K. K., Christiansen, J. L., et al. 2021, AJ, 162, 259, doi: [10.3847/1538-3881/ac2309](https://doi.org/10.3847/1538-3881/ac2309)
- Zurlo, A., Cieza, L. A., Pérez, S., et al. 2020, MNRAS, 496, 5089, doi: [10.1093/mnras/staa1886](https://doi.org/10.1093/mnras/staa1886)